

TPV: Parameter Perturbations Through the Lens of Test Prediction Variance

Devansh Arpit¹

Abstract

We identify *test prediction variance* (TPV)—the first-order sensitivity of model outputs to parameter perturbations around a trained solution—as a unifying quantity that links several classical observations about generalization in deep networks. TPV is a fully label-free object whose trace form $\text{Tr}(H_{\text{eff}}C)$ separates the geometry of the trained model H_{eff} from the specific perturbation mechanism C , allowing a broad family of parameter perturbations like SGD noise, label noise, finite-precision noise, and other post-training perturbations to be analyzed under a single framework.

Theoretically, we show that TPV estimated on the training set converges to its test-set value in the overparameterized limit, providing the first result that prediction variance under local parameter perturbations can be inferred from training inputs alone. Empirically, TPV exhibits a striking stability across datasets and architectures—including extremely narrow networks—and correlates well with clean test loss.

Finally, we demonstrate that modeling pruning as a TPV perturbation yields a simple label-free importance measure that performs competitively with state-of-the-art pruning methods, illustrating the practical utility of TPV. [Code Here](#)

1. Introduction

Despite remarkable empirical success, our understanding of why modern deep networks generalize—even in heavily overparameterized and noise-perturbed regimes—remains incomplete. Several perspectives have been proposed—wide minima (Hochreiter & Schmidhuber, 1997; Keskar & et al., 2017), implicit optimization bias (Mandt et al., 2017; Smith & Le, 2018; Chaudhari & Soatto, 2018; Soudry et al., 2018; Zhang et al., 2017), benign overfitting in overparameterized networks (Belkin et al., 2019; Bartlett et al., 2020;

¹Modelable AI. Correspondence to: Devansh Arpit <devansharpit@gmail.com, devansh@modelable.ai>.

Preprint version.

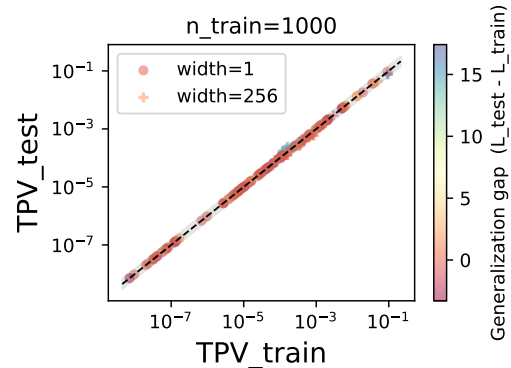


Figure 1. TPV stability on synthetic data: Each point corresponds to one synthetic configuration (dataset type, input dimension, network width, depth) and one perturbation source (label noise; SGD noise). Axes show empirical TPV on the training and test sets; $y = x$ is the ideal reference line along with a gray colored 50% error band; colormap indicates generalization gap $L_{\text{test}} - L_{\text{train}}$. We ran 324 configurations from label-noise and SGD-noise, spanning more than five orders of magnitude in TPV and different levels of generalization gaps. Despite this heterogeneity, all points concentrate tightly around the diagonal $\text{TPV}_{\text{train}} = \text{TPV}_{\text{test}}$; most surprisingly, even for $\text{width} = 1$. This demonstrates that: i) TPV stability holds true even at extremely low widths; ii) TPV stability is decoupled from generalization. See section 5.1 for more experiments.

Belkin et al., 2020), and Neural Tangent Kernel (NTK) (Jacot et al., 2018; Adlam & Pennington, 2020a), to name a few. While each viewpoint explains part of the puzzle, they rely on different analytical lenses and seldom yield a single quantity that directly predicts test-set behavior for a *fixed, trained model* subject to realistic perturbations.

Deep networks deployed in practice are almost never evaluated based on the variability induced by the *entire training process*. Rather, we care about stochastic gradient noise near convergence, finite-precision arithmetic, label noise during fine-tuning, structured reparameterizations, or post-training modifications such as pruning. All of these processes act *locally* around an already-trained solution w^* rather than by retraining from scratch. This motivates a shift in emphasis from global notions of prediction variability to a *local* quantity that measures the test sensitivity of $f(x; w^*)$.

We formalize this sensitivity through the *test prediction*

variance (TPV): the local variance of a trained model’s predictions under parameter perturbations. Crucially, note that this is different from global prediction variance (see Section 2). Under a first-order approximation, TPV reduces to a compact trace form

$$\text{TPV}(w) \approx \text{Tr}(H_{\text{eff}} C), \quad (1)$$

where H_{eff} is second moment of the output-parameter Jacobian and $C = \mathbb{E}[\delta w \delta w^\top]$ is the perturbation covariance. This decomposition separates a *label-free geometric factor* H_{eff} from the *noise mechanism* encoded in C and reveals that diverse perturbations—including SGD noise, label noise, quantization noise, and pruning masks—all influence test predictions through the same curvature–covariance interaction. Variants of $\text{Tr}(H_{\text{eff}} C)$ appear in analyses of SGD dynamics (Zhu et al., 2018; Thomas et al., 2020; Bar et al., 2024). However, prior work does not interpret this object as a *predictive variance functional* nor use it as a unifying lens for heterogeneous real-world perturbations.

Our key observation is that each of these noise mechanisms can be well-approximated, near minima, as inducing small zero-mean parameter perturbations. Once this modeling step is accepted, the first-order TPV expression applies uniformly: all such perturbations act through the same geometric factor H_{eff} and differ only in their noise covariance C . Our contributions are as follows:

1. **Test Prediction Variance (TPV) as a unified perturbation lens:** We formalize TPV as a local prediction-variance functional and show that SGD noise, label noise, quantization, and pruning all influence test robustness through the same trace form $\text{Tr}(H_{\text{eff}} C)$.
2. **TPV Trace Stability:** We prove that, in overparameterized networks, training-set TPV converges to test-set TPV, providing the first theoretical result showing that logit prediction variance under parameter perturbations, when evaluated on training-set inputs, is a reliable test-time estimator. Empirically, we find that TPV stability holds true even at very low widths and only breaks if either the number of samples are low or the first order approximation is broken by perturbations.
3. **Correlation with Test Loss:** We find that empirical TPV estimates correlate well with test loss. Together with TPV stability, it provides a new way to gauge generalization and robustness using training dataset at a granular level by plugging in specific noise mechanisms.
4. **Applications to label noise, SGD noise, and pruning.** We derive TPV expressions for label noise and SGD stationary noise, reveal how overparameterization and wide minima suppresses prediction variance, and introduce JBR—a practical pruning criterion derived from

TPV geometry—that matches or exceeds state-of-the-art baselines on CIFAR-10/100 and ImageNet.

2. Test Prediction Variance

Classical bias–variance analyses (Geman et al., 1992; Friedman, 1997) study the *global* prediction variance $\text{Var}_w[f_w(x)]$ obtained by retraining the model under different sources of randomness (e.g., parameter initialization, stochastic gradient noise, stochastic regularization such as dropout). For instance, Neal et al. (2018) revisit this global notion for deep networks, analyzing the variability induced by initialization, data sampling, and optimization. Accordingly, global variance provides insight into properties of the *learning algorithm*—such as algorithmic stability, the double descent phenomenon, and the benefits of ensembling.

In contrast, our test prediction variance (TPV) is a *localized* quantity that measures the effect of infinitesimal weight-space perturbations around a *fixed* solution w^* :

$$\text{TPV} := \mathbb{E}_{x, \delta w} \left[\|f_{w^* + \delta w}(x) - f_{w^*}(x)\|^2 \right]. \quad (2)$$

This local perspective is more directly appropriate for understanding robustness to realistic noise sources near or after convergence—label noise at convergence, SGD stationary noise, quantization noise, dropout during inference, and post-training pruning masks—all of which act as *perturbations around a trained model* rather than as full retraining procedures.

Crucially, TPV conditions on a particular trained solution w^* , whereas global variance averages over the entire distribution of solutions obtainable by the learning algorithm. The two quantities therefore capture fundamentally different notions of variability.

We now formalize test prediction variance and derive a compact spectral expression that will be reused in all settings.

2.1. Our starting point: expected test error variance

We posit that the relevant quantity is the *expected test error* of the trained model w^* , decomposed into a model-bias term and a *test prediction variance* term that captures the effect of small parameter perturbations around w^* .

Let δw denote a zero-mean parameter perturbation drawn from a distribution R that models the sources of noise acting near or after convergence (label noise at convergence, SGD stationary noise, finite precision, pruning masks, etc.), denote its covariance matrix by $C := \mathbb{E}_R[\delta w \delta w^\top] \in \mathbb{R}^{p \times p}$. The perturbed predictor is $f_{w^* + \delta w}$. For a test pair (x, y) with $y = f^*(x)$, the expected test error is

$$\mathcal{E}_{\text{test}} = \mathbb{E}_{x, y, R} [(f_{w^* + \delta w}(x) - y)^2].$$

Expanding this quantity and using $\mathbb{E}_R[\delta w] = 0$ gives the decomposition

$$\mathcal{E}_{\text{test}} = \text{TPV} + \underbrace{\mathbb{E}_x[(f_{w^*}(x) - f^*(x))^2]}_{\text{bias}^2}. \quad (3)$$

where for a fixed test point x , we assume $f_w(x)$ is smooth in w and linearize around w^* :

$$f_{w^* + \delta w}(x) \approx f_{w^*}(x) + J(x)\delta w, \quad (4)$$

where

$$J(x) := \nabla_w f_{w^*}(x) \in \mathbb{R}^{1 \times p} \quad (5)$$

is the Jacobian of the model output with respect to parameters at w^* .

Under this approximation,

$$\begin{aligned} \text{TPV} &\approx \mathbb{E}_{x,R}[(J(x)\delta w)^2] \\ &= \mathbb{E}_{x,R}[\text{Tr}(J(x)^\top J(x)\delta w\delta w^\top)] \\ &= \text{Tr}(\mathbb{E}_x[J(x)^\top J(x)]\mathbb{E}_R[\delta w\delta w^\top]) \\ &= \text{Tr}(H_{\text{eff}}C), \end{aligned} \quad (6)$$

where

$$H_{\text{eff}} := \mathbb{E}_x[J(x)^\top J(x)] \quad (7)$$

is the second moment of the Jacobian. Note that H_{eff} is not the Hessian in general, though it does become equivalent to the Hessian under special circumstances. Further, note that H_{eff} is taking expectation on the test distribution, while the second moment of the parameter perturbations C either depends on the training dataset (e.g. label noise, SGD stationary noise) or is data-agnostic (e.g. quantization).

Eq. (6) is the central object in this paper: TPV, and in turn the expected test error (due to Eq. (3)), is controlled by the interaction between the curvature spectrum of H_{eff} and the perturbation covariance C .

2.2. TPV Trace Stability

In this section, we prove that for trained overparameterized networks of width $m \rightarrow \infty$, TPV estimated entirely using the training dataset acts as a good estimator of the test set TPV object.

Denote by $X_{\text{tr}} = \{x_i\}_{i=1}^n$ and $X_{\text{te}} = \{x_i\}_{i=1}^{n_{\text{te}}}$ training and test datasets sampled i.i.d. from the same underlying data distribution \mathcal{D} . Let w^* be the parameter vector obtained after training a deep network of width m on X_{tr} . We denote the estimator of H_{eff} on the dataset $X \in \{X_{\text{tr}}, X_{\text{te}}\}$ as:

$$H_{\text{eff}}(w^*; X) := \frac{1}{|X|} \sum_{x_i \in X} J(x_i; w^*)^\top J(x_i; w^*).$$

Theorem 2.1 (TPV Trace Stability). *The following upper-bound holds for over-parameterized networks:*

$$|\text{TPV}(w^*; X_{\text{tr}}) - \text{TPV}(w^*; X_{\text{te}})| \leq c_1 \text{Tr}(C). \quad (8)$$

where $c_1 := (2\varepsilon_{\text{NTK}} + o_{n_{\text{tr}}, n_{\text{te}}}(1))$ and C is the parameter perturbation covariance matrix, such that $\varepsilon_{\text{NTK}} \rightarrow 0$ as $m \rightarrow \infty$ and $o_{n_{\text{tr}}, n_{\text{te}}}(1) \rightarrow 0$ as $n, n_{\text{te}} \rightarrow \infty$.

See Appendix A for proof. This result is important because it shows that, in sufficiently overparameterized networks, the TPV estimate $H_{\text{eff}}(w^*; X_{\text{tr}})$ and equivalently Eq. 2 (under the first order approximation) estimated using the training set already carries enough information to approximate the test-set TPV that governs test prediction variance.

The intuition behind the proof is simple and uses two observations—1. Jacot et al. (2018); Allen-Zhu et al. (2019) show that the NTK kernel remains stable during training; 2. due to random initialization and i.i.d. sampling of datasets, $H_{\text{eff}}(w_0; X)$ concentrates around its population counterpart in operator norm for both X_{tr} and X_{te} due to the Law of Large Numbers. Combining these two observations allows us to upper-bound the distance between the training set and test set TPV objects. We use this assumption in section 3.2 and 3.3.

3. Parameter Perturbation Sources

In this section, we study the effect of individual noise sources in isolation on test prediction variance (TPV). Specifically, we revisit label noise, SGD mini-batch noise, and finite-precision noise, and show how the benefits of over-parameterization and wide minima arise from the common mechanism of suppressing TPV.

3.1. Label Noise

In this section, we do not invoke the TPV trace stability result and study the TPV object in its general form.

Linear Case

Remark 3.1 (TPV in Linear Case). Let the training labels be generated as $y_i = \theta^* x_i + \varepsilon_i$, where $\varepsilon_i \sim \mathcal{N}(0, \sigma_\varepsilon^2)$ are i.i.d. label-noise variables, and denote by $X \in \mathbb{R}^{n \times d}$ the training dataset matrix containing n samples of dimension d . Assume: (i) $d \geq n$ and X has full row rank, (ii) the data distribution is whitened so that $\mathbb{E}_x[xx^\top] = I_d$, and (iii) θ^* lies in the row span of X . Let w^* be a minimizer of the empirical linear regression loss using SGD. Then the TPV under linear regression is given by,

$$\text{TPV}_{\text{label}} = \sigma_\varepsilon^2 \text{Tr}((XX^\top)^{-1}). \quad (9)$$

The proof is shown in Appendix B for completeness. Note that in the linear regression setting above, the “global” pre-

diction variance $\mathbb{E}_x \text{Var}_\varepsilon(f_{w^*}(x))$ obtained by retraining on different noisy label realizations coincides exactly with the *local* TPV quantity $\text{Tr}(H_{\text{eff}}C)$, and is a well known result (Bartlett et al., 2020) in literature characterizing benign overfitting in linear regression models. This is because the conditioning of the matrix XX^\top improves as d grows beyond n , resulting in lower $\text{TPV}_{\text{label}}$, making the model less sensitive to label noise. Even more specifically, if training and test distributions are identical, then for a large enough $n(\ll d)$, we have $\frac{1}{n}X^\top X = I_d$ (due to the whitening assumption). Under isotropic/whitened assumptions on the rows of X , random matrix theory (Wishart) gives $\mathbb{E}(XX^\top)^{-1} \approx \frac{1}{d}I_n$. Therefore, $\text{TPV}_{\text{label}} \approx \sigma_\varepsilon^2 n/d$.

Non-Linear Case

Theorem 3.2 (TPV in Non-Linear Case). *Let the training labels be generated as $y_i = f_{\theta^*}(x_i) + \varepsilon_i$, where f_{θ^*} is any fixed target function and ε_i are i.i.d. zero-mean noise variables with variance σ_ε^2 . Let w^* be a parameter vector of the network satisfying $f_{w^*}(x_i) = f_{\theta^*}(x_i)$ for all training inputs. Under the first-order approximation of the network around w^* , let $w^* + \delta w$ be a stationary point of the MSE loss w.r.t. δw when training on the noisy labels $y_i = f_{\theta^*}(x_i) + \varepsilon_i$ in this linearized model. If δw is chosen to be the **minimum-norm stationary point**, then the expected test prediction variance due to label noise is,*

$$\text{TPV}_{\text{label}} \approx \sigma_\varepsilon^2 \sum_{i=1}^r \frac{B_{ii}}{s_i^2}, \quad (10)$$

where:

- s_i 's ($i \in [r]$) are the nonzero singular values of the output-parameter Jacobian J evaluated on the training set,
- B_{ii} denotes the i -th diagonal entry of $B := V^\top H_{\text{eff}} V$, where V contains the right singular vectors of J , and H_{eff} depends on the test distribution

The proof is provided in Appendix C. Equation 10 expresses the contribution of label noise to test prediction variance as a spectral sum involving (i) test-distribution Jacobian modes B_{ii} and (ii) the corresponding training singular values s_i . The linear result (Eq. 9) is a special case of Eq. 10 when the nonlinear Jacobian is replaced by the data matrix. To our knowledge, Eq. 10 is the first expression of label-noise-induced prediction variance for finite-width deep networks in terms of a test-Jacobian operator and a general parameter-noise covariance C , that also accommodates other perturbation sources (e.g., SGD noise, finite precision, pruning masks) within the same $\text{Tr}(H_{\text{eff}}C)$ template.

Equation 10 highlights that label-noise sensitivity is dominated by directions where B_{ii} is large while s_i is small—i.e.,

where the test-distribution Jacobian aligns with poorly conditioned training directions. This makes explicit how the *local geometry* around w^* —particularly the conditioning and alignment of Jacobian modes—governs test-prediction variance.

Connection to Over-Parameterization and Benign Overfitting. Theorem 3.2 shows that TPV under label noise depends fundamentally on the *local conditioning* of the Jacobian at w^* . However, over-parameterization matters because, in many modern training regimes, it induces solutions whose Jacobians are well-conditioned. This phenomenon has been rigorously studied through Neural Tangent Kernel (NTK) theory.

Let $J(w) \in \mathbb{R}^{n \times p}$ denote the Jacobian of network outputs on the n training points and let $G(w) = J(w)J(w)^\top$ be the empirical NTK matrix. When $p \gg n$, the non-zero singular values of $J(w)$ correspond to the eigenvalues of $G(w)$. For two-layer ReLU networks, Du et al. (2018) show that with sufficient width, the smallest eigenvalue $\lambda_{\min}(G(w_0))$ is bounded away from zero at initialization and remains so during training. Bombari et al. (2022) extend this to deep networks with $\Omega(n)$ parameters, establishing well-conditioned NTK structure at initialization. Moreover, Allen-Zhu et al. (2019) prove that SGD remains in a neighborhood of initialization where the NTK matrix stays close to its well-conditioned initial value.

Consequently, in the overparameterized regime, the non-zero singular values of $J(w)$ remain bounded away from zero, suppressing the $\frac{B_{ii}}{s_i^2}$ terms in Eq. 10 and thereby yielding lower label-noise TPV. In this sense, over-parameterization and benign overfitting can be interpreted through the TPV lens: they steer optimization toward regions of the loss landscape with stable Jacobian geometry, which reduces test prediction variance.

Pathological Cases Two pathological regimes are worth noting w.r.t. Eq. 10. (i) When the linearized system around w^* interpolates the noisy labels (e.g., $J\delta w = \varepsilon$ with full row rank), both the training TPV and the label-noise TPV in Eq. 10 collapse to σ_ε^2 (or to 0 as $\sigma_\varepsilon^2 \rightarrow 0$) if the training and test distributions match. TPV stability then holds trivially, but TPV becomes uninformative across architectures. (ii) When σ_ε^2 is sufficiently large that the noisy solution leaves the linearization regime, the assumptions of Theorem 3.2 no longer apply and the label-noise TPV formula should not be used. The non-degenerate, small-but-finite noise regime—where **interpolation does not occur and the linear approximation remains valid, and the minimum solution is achieved**—is the regime in which label noise TPV exhibits meaningful geometric dependence and is useful. On a related note, SGD in deep networks may not find the min-norm solution in δw and is a proxy for the

true optimization problem. See Appendix C.2 and C.3 for a detailed discussion on the label noise TPV object.

3.2. SGD Stationary Noise Near Convergence

Theorem 3.3 (TPV under SGD Noise). *Consider a scalar-output non-linear model $f(x; w)$ trained using SGD with squared loss L on a fixed dataset $\{(x_i, y_i)\}_{i=1}^n$ sampled i.i.d. from an underlying distribution \mathcal{D} without any label noise, and assume that there exists a minimizer w^* that achieves zero training loss. Then,*

$$\boxed{\text{TPV}_{\text{SGD}} \approx \frac{\eta\sigma_\varepsilon^2}{2b} \text{Tr}(\nabla_w^2 L(w^*))} \quad (11)$$

where, η and b are the SGD learning rate and batch size, and σ_ε^2 denotes the variance of the residual error over the training samples induced by mini-batch gradient noise.

The proof is shown in Appendix D and invokes the TPV trace stability result because we use H_{eff} computed on the training set.

Connection to Wide-minima Hypothesis: There has been much debate on whether or not the flatness of minima affects the generalization performance of the final model achieved at the end of the training process. The classic counter-argument against the wide-minima hypothesis by Dinh et al. (2017) is that by reparameterizing the weights of a network, the spectrum of the Hessian can be changed without changing the input-output function map.

However, in reality, noise sources like SGD mini-batch or finite precision prevent the weights from reaching w^* precisely. Theorem 3.3 shows that small perturbations in parameters due to a fixed SGD noise (η/b) in a sharp basin make the TPV (and in turn test error) large; thus, SGD effectively samples from a high-variance region of the loss surface, leading to unstable test behavior and degraded generalization despite low training error.

3.3. Finite-precision noise

Remark 3.4 (TPV under Quantization Noise). Consider a scalar-output non-linear model $f(x; w)$ trained using GD (not SGD) with squared loss L on a fixed dataset $\{(x_i, y_i)\}_{i=1}^n$ sampled i.i.d. from an underlying distribution \mathcal{D} without any label noise, and assume that there exists a minimizer w^* that achieves zero training loss. Then,

$$\boxed{\text{TPV}_{\text{quant}} \approx \frac{\delta^2}{12} \text{Tr}(\nabla_w^2 L(w^*))} \quad (12)$$

where, $\text{Var}(\delta w_j) = \delta^2/12$ denotes each parameter’s variance under quantization under a simple independent per-coordinate quantization model,

$$\delta w_j \sim \text{Unif}(-\delta/2, \delta/2), \forall j \in [p]$$

The proof is shown in Appendix E. Thus, similar to section 3.2, the above claim shows that sharper minima increase generalization error under quantization/finite precision.

3.4. Jacobian-Based Rebalancing (JBR) for Pruning

We adopt the viewpoint that pruning should preserve the model’s predicted class on the correctly classified training samples. For a classifier with logits $f(x; w) \in \mathbb{R}^K$, the full logit vector is irrelevant for this purpose; prediction changes only if the probability of the currently predicted class drops relative to the others. Thus, instead of treating f itself as the task in the TPV framework, we work with the scalar functional

$$u(x; w) := -\log(p_{c(x)}(x; w)),$$

where $c(x) := \arg \max_k p_k(x; w^*)$ and $p = \text{softmax}(f)$ and w^* is the reference (unpruned) network. This quantity uses the probability assigned to the class the model originally predicted, and pruning should leave this value stable. Specifically, we only want to include training samples for which the model predicts correctly. As a proxy, we select samples for which $p_{c(x)}(x; w) > \tau$, where τ is a probability threshold (we use $\tau = 0.9$). We caution that the TPV Trace Stability theorem only applies to logits ($f(\cdot)$) and does not directly apply to functionals like $u(\cdot)$ considered above. We leave that analysis for future work. The focus here is to formulate pruning score as a TPV object.

Pruning as a Source of Parameter Noise Once training has converged and we are interested purely in pruning, the dominant source of parameter perturbation is the pruning operation itself. In many practical settings we prune entire groups at once (e.g., channels). Define $g \subseteq \{1, \dots, p\}$ as a group with parameter vector $w_g \in \mathbb{R}^{p_g}$, and for a given group g we either prune all its parameters or keep them all. We model pruning as a structured parameter perturbation that acts coherently on each parameter group. For sensitivity analysis within the TPV framework, we introduce a zero-mean, group-aligned perturbation:

$$\delta w_g = \sigma \xi_g w_g, \quad g \in \mathcal{G}, \quad (13)$$

where $\sigma > 0$ is a small scalar controlling the perturbation scale and ξ_g is a Rademacher random variable taking values ± 1 with equal probability. Thus $\mathbb{E}[\delta w_g] = 0$ and the group-wise pruning covariance is

$$C_{\text{prune},g} := \mathbb{E}[\delta w_g \delta w_g^\top] = \sigma^2 w_g w_g^\top. \quad (14)$$

Treating masks as being independent across groups, the full pruning covariance C_{prune} is block-diagonal with blocks $\{C_{\text{prune},g}\}_{g \in \mathcal{G}}$. Using the cyclic property of the trace, the contribution of group g to the TPV object is

$$\text{Tr}(H_{\text{eff},g} C_{\text{prune},g}) = \sigma^2 \cdot \mathbb{E}[w_g^\top J_{u,g}^\top J_{u,g} w_g]. \quad (15)$$

where $J_{u,g}(x; w) := \partial u(x; w) / \partial w_g \in \mathbb{R}^{1 \times p_g}$. Thus, to keep the overall TPV low for a pruned network, we want to set $\sigma^2 = 0$ for groups with large $w_g^\top J_{u,g}^\top J_{u,g} w_g$ and only prune groups (equivalently $\sigma^2 > 0$) with small $w_g^\top J_{u,g}^\top J_{u,g} w_g$. Thus we define the JBR importance of a parameter group as

$$\boxed{\text{score}_{\text{JBR}}(w_g) := \mathbb{E}_x [w_g^\top J_g^\top \delta_u^\top \delta_u J_g w_g]}. \quad (16)$$

where $J_g := \partial f(x; w) / \partial w_g \in \mathbb{R}^{K \times p_g}$, and $\delta_u := \partial u(x; w) / \partial f(x; w) \in \mathbb{R}^K$.

Connection and Contrast with JC The proposed JBR is very similar to Jacobian Criterion (JC) proposed by (Chen et al., 2025) and can be seen as a label-free version of JC. Both JBR and JC assign a score to each parameter group g of the form

$$\begin{aligned} \text{score}(w_g) &= \mathbb{E}_x [w_g^\top J_g(x)^\top m(x) m(x)^\top J_g(x) w_g] \\ &= \mathbb{E}_x [(m(x)^\top v_g(x))^2], \end{aligned}$$

where $v_g(x) = J_g(x) w_g$ is the logit-space direction induced by group g , and the only difference between the two methods lies in the choice of the logit-space vector $m(x)$:

$$\begin{aligned} m_{\text{JC}}(x) &:= \delta_L(x) = p(x) - y(x), \\ m_{\text{JBR}}(x) &:= \delta_u(x) = p(x) - e_{c(x)}. \end{aligned}$$

To understand the relationship between JC and JBR clearly, consider the clean setting in which all the labels in the training data are correct. Now, if the trained (unpruned) model predicts all the training samples correctly, then $y(x) = e_{c(x)}$, and JBR and JC importance scores become identical. The scores differ when either: i) the labels used in JC have noise; or, ii) the model predicted class labels used in JBR are incorrect.

4. Relation to prior work

4.1. Test Prediction Variance

Work on double descent and benign overfitting explains how heavily overparameterized models can interpolate noisy data yet still generalize, typically by analyzing the test risk of minimum-norm or ridgeless interpolators as a function of model capacity or feature spectrum (Belkin et al., 2019; Bartlett et al., 2020). This line of work focuses on global risk curves and asymptotic regimes, rather than on how small parameter perturbations around a fixed trained model translate into test prediction variance.

Work on implicit optimization bias studies how training dynamics alone can select particular predictors among many interpolating solutions, for example modeling SGD as a stochastic process that samples from a local Gibbs/posterior

distribution (Mandt et al., 2017; Smith & Le, 2018; Chaudhari & Soatto, 2018) or showing that (stochastic) gradient descent on separable problems converges to max-margin classifiers in function space (Soudry et al., 2018), or the implicit bias of SGD towards solutions that generalize well (Zhang et al., 2017; Rahaman et al., 2019; Xu et al., 2019). These works focus on characterizing the solutions and stationary distributions implicitly favored by the optimizer. Similarly, classical work on wide/flat minima (Hochreiter & Schmidhuber, 1997; Keskar & et al., 2017) and related sharpness-aware training methods such as SAM (Foret et al., 2020) are concerned with how the geometry of the loss landscape—typically measured through Hessian eigenvalues or sharpness—correlates with generalization. These approaches focus on the selection process of wide versus flat minima and how optimization affects this choice. The TPV framework analyzes how curvature interacts with parameter perturbation covariance for a trained model for arbitrary perturbation sources and links local parameter sensitivity to test-time behavior.

Classical bias–variance analyses decompose prediction error into contributions from the mean predictor and its variability manifested by retraining the model on different training sets and other sources of randomness (Geman et al., 1992; Friedman, 1997; Neal et al., 2018). More recently, Bordelon & Pehlevan (2023) analyze the prediction fluctuations in finite-width networks using dynamical mean-field theory to characterize how test prediction variance arises from kernel fluctuations during training. In contrast to these global decompositions of test risk, our TPV framework focuses on a local prediction-variance functional around a fixed trained model, quantifying how curvature and parameter perturbation covariance jointly control test prediction variance.

There is also research on bias–variance decomposition that studies how the two components correlate in modern deep learning. Neal et al. (2018) show that, as network width grows, both the global bias and variance components of test error can decrease together, contradicting the textbook U-shaped trade-off. Yang et al. (2020) similarly find monotonically decreasing bias and a unimodal (bell-shaped) variance curve in width, so that in the overparameterized regime risk is largely controlled by bias. A complementary random-feature study by Adlam & Pennington (2020b) provides a fine-grained global bias–variance decomposition and identifies regimes where both terms become small. In contrast, our TPV formulation investigates a fundamentally different phenomenon: a *local*, perturbation-based variance (TPV) *around a fixed trained reference model*, exhibits a systematic correlation with clean test error.

Work on the Neural Tangent Kernel (NTK) shows that, in the infinite-width limit, gradient descent training of neural networks is equivalent to kernel regression with a fixed

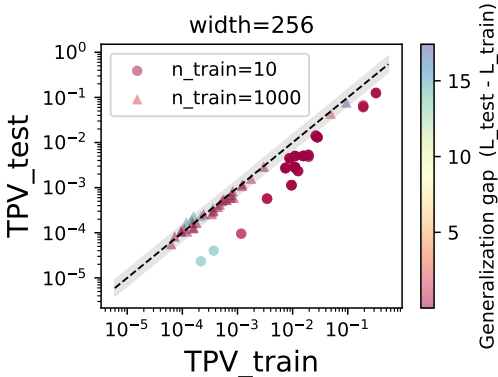


Figure 2. **TPV stability on synthetic data:** Analogous to Figure 1, Each point corresponds to one synthetic configuration and one perturbation source. We ran 324 configurations. In Figure 1, we fixed the number of training samples $n_{\text{train}} = 1000$ and varied network width. In this experiment, we fixed width to 256, and vary n_{train} . We find that **TPV stability breaks when n_{train} is too low** (10; circles)— points are far outside the gray 50% error band, but holds for sufficiently large n_{train} .

kernel, yielding precise characterizations of training dynamics and generalization in terms of the NTK spectrum (Jacot et al., 2018; Lee et al., 2019; Arora et al., 2019). Our TPV framework leverages this infinite-width NTK regime to obtain a trace-stability theorem—showing that $\text{Tr}(H_{\text{eff}} C_{\text{prune}})$ computed on training set converges to the test set estimate—while providing a curvature-covariance interpretation of prediction variance applicable to finite networks as well.

4.2. Pruning

Pruning aims at reducing model size and improving inference speed (LeCun et al., 1989; Hassibi et al., 1993). These methods can be broadly categorized into unstructured and structured pruning.

Unstructured pruning removes each parameter individually (Han et al., 2015; Wang et al., 2020; Frankle & Carbin, 2018; Paul et al., 2022). While this approach aligns with the goal of reducing model size, it often does not significantly boost inference speed. Structured pruning (Molchanov et al., 2019; Liu et al., 2021), on the other hand, removes entire neurons, filters, or attention heads, resulting in models that are easier to accelerate on standard hardware.

Structured pruning can be further divided into data-dependent and data-independent pruning. Data-independent strategies typically rely on pretrained weight statistics; removing groups with small parameter norm (Li et al., 2017), BatchNorm scale (Liu et al., 2017), or geometric and structural properties of the pretrained weights—such as norms, redundancy, clustering, or subspace contribution—to estimate filter importance without relying on labels or loss gradients (He et al., 2019; Singh et al., 2020; Chen et al., 2023).

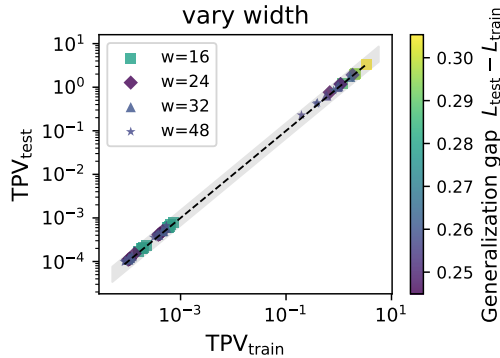


Figure 3. **TPV stability on CIFAR-10:** Analogous to Figure 1, this scatter plot shows that **TPV stability holds for architectures with different widths** on CIFAR-10.

Data-dependent strategies on the other hand prune parameter groups based on the sensitivity of loss w.r.t. neurons or parameters. The sensitivity can be estimated in different ways—second order approximation (Liu et al., 2021), Fisher approximation (Theis et al., 2018), and first order approximation (You et al., 2019; Molchanov et al., 2016; 2019; Chen et al., 2025).

The proposed JBR pruning strategy is particularly close to Jacobian Criterion (JC) (Chen et al., 2025). The key difference is that JC measures loss sensitivity w.r.t. parameter groups using ground-truth labels under the first order approximation, while JBR measures loss sensitivity using the model predicted class labels for confident samples. Under the specific scenario where ground-truth labels are fully correct and model predictions are fully accurate on the training samples, the two become equivalent. The main motivation behind JBR is that it models pruning as a special case of parameter perturbation noise under the general TPV framework.

5. Experiments

We run experiments around TPV stability between training and test sets and empirically identify the conditions when it holds and when it breaks. We then study TPV under label noise and how width plays an important role in modulating it. We do not include experiments for SGD based perturbations and the relation between the flatness of minima and TPV because several prior research works have confirmed a similar relationship (Keskar & et al., 2017; Smith & Le, 2018; Jastrzebski et al., 2017). Finally, we run experiments on the proposed JBR pruning algorithm comparing its performance to existing post-training pruning methods.

5.1. TPV Stability

Theorem 2.1 states that under the first order approximation of Eq. 2, TPV estimated using training set should be close to the test set TPV when the network width approaches infinity

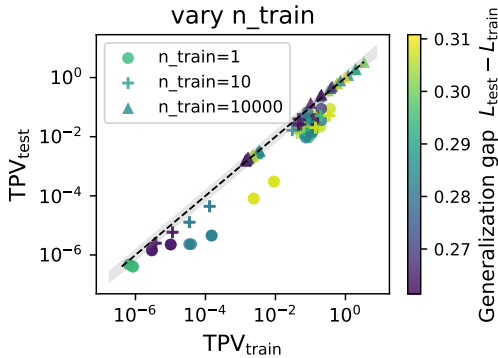


Figure 4. **TPV stability on CIFAR-10:** Analogous to Figure 2, this scatter plot shows that **TPV stability breaks for very low values of n_{train}** and holds increasingly better (close to $y = x$ line and within the 50% error band) for larger values.

and the number of training samples is large enough. The former condition arises due to the fact that we use NTK stability assumption in our proof, which assumes extremely wide networks. The latter condition arises due to the application of the Law of Large Numbers applied at initialization. In the experiments in this section, instead of the trace form of TPV in Eq. 6, we use the original form in Eq. 2.

When estimating TPV using Eq. 2, we find to our surprise that the former condition is hardly required, i.e., TPV stability seems to hold quite tightly in the experiments— even at width = 1 in the synthetic data experiments, and only breaks when the number of samples used for estimation are too low. Experiments on CIFAR-10 make a similar case.

Synthetic data: To stress-test TPV trace stability beyond any single model or dataset, we construct a large synthetic benchmark spanning a broad grid of architectures, data distributions, and perturbation sources. We perform two sets of experiments— in the first experiment, we fix network width in $\{1, 256\}$ and for each width experiment with all combinations of the other configurations; in the second experiment, we fix the number of training samples in $\{10, 10000\}$ and do the same. In each set, there are a total of 324 distinct experiments (each with 20 independent runs). For each combination, we first train a clean reference network f_{w^*} on noiseless regression targets. Around each such f_{w^*} , we then instantiate two different parameter-noise mechanisms— label noise and SGD stationary noise— and train independent copies of the reference network under these noise mechanisms and get a perturbed version of the network. Importantly, we discard the runs that violate the first order assumption (using a simple finite-difference approximation check) and in which noisy model loss does not go down. For full details, see Appendix F.1.

For each configuration we estimate the empirical TPV on

the training set X_{tr} and test set X_{te} ,

$$\text{TPV}_X = \mathbb{E}_{r, x \sim X} \left[(f_{w^* + \delta w(r)}(x) - f_{w^*}(x))^2 \right]. \quad (17)$$

where $X \in \{X_{\text{tr}}, X_{\text{te}}\}$. X_{te} always contains 5000 samples. We plot the two estimates against each other on a log–log scale (Figure 1) for X_{tr} with 1000 samples and vary width. Each point is colored by the generalization gap of the clean model, $L_{\text{test}} - L_{\text{train}}$, and uses a different marker for label noise versus SGD noise. In the resulting unified scatter plot, TPV values span more than five orders of magnitude, yet the cloud of points lies in a remarkably tight band along the diagonal— $\text{TPV}_{\text{train}} \approx \text{TPV}_{\text{test}}$.

In Figure 2, we run the same experiment as above, except we now fix network width to be 256, and only vary the number of samples in X_{tr} in $\{10, 1000\}$. We now see that TPV stability breaks (points far from diagonal and outside the 50% error band) when $n_{\text{train}} = 10$ but holds tightly for $n_{\text{train}} = 1000$.

CIFAR-10/100: We now verify TPV stability on CIFAR-10 dataset. Similar to the synthetic data experiment above, we first use architectures of different widths and fix the number of training samples. The scatter plot is shown in Fig. 3. Similar to Fig. 1, TPV remains stable across different widths.

We next study the effect of the number of training samples. The scatter plot is shown in Fig. 4. Once again, we find that TPV stability breaks when n_{train} is extremely low ($n_{\text{train}} = 1$ lies outside the 50% error band), holds better for $n_{\text{train}} = 10$ (mostly within the band), and very tightly for $n_{\text{train}} = 10000$. Analogous experiments on CIFAR-100 are shown in Fig. 11 and 12 in the Appendix. Full experimental details are in Appendix F.1.2.

Interpretation : We make three important observations from these experiments: i) points corresponding to large generalization gaps are just as close to the diagonal as those with small gaps as long as we use a large n_{train} . This shows that empirical TPV computed using training and test sets match closely irrespective of the generalization performance of the model. We call this TPV stability¹. Therefore, TPV stability is decoupled from generalization; ii) TPV stability holds even when network width is very small; iii) TPV stability breaks when the number of samples used for estimation is too small.

5.2. Empirical Evaluation of TPV Under Label Noise

We now empirically study the TPV term appearing in Theorem 3.2. Recall that for additive zero-mean label noise with

¹TPV stability is different from TPV trace stability since former uses Eq. 2 while the latter uses Eq. 6.

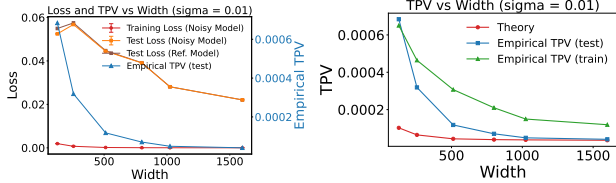


Figure 5. Empirical and theoretical TPV estimates under label noise on synthetic data for noise standard deviation $\sigma = 0.01$. As width increases, both TPV estimates reduce. Further, TPV correlates with test loss.

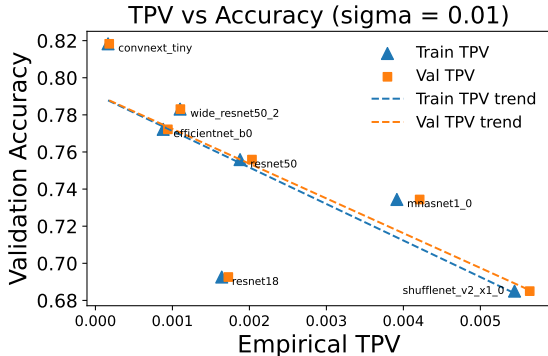


Figure 6. Empirical TPV estimates under label noise on Imagenet for noise standard deviation $\sigma = 0.01$. TPV stability holds and models that generalize better typically have lower TPV estimates.

variance σ_ϵ^2 , the label-noise contribution to test prediction variance is $\text{TPV}_{\text{label}} \approx \sigma_\epsilon^2 \sum_{i=1}^r \frac{B_{ii}}{s_i^2}$, where B_{ii} depends on test-distribution Jacobian modes and s_i are the singular values of the training-set Jacobian. For sufficiently small noise variance, the multiplicative factor $T_{\text{base}} := \sum_{i=1}^r \frac{B_{ii}}{s_i^2}$ fully determines label-noise sensitivity of the model at w^* . As discussed in Section 3.1, T_{base} depends on the *local Jacobian geometry* around the reference model. Width nevertheless provides a convenient dial that often moves optimization trajectories into different geometric regimes.

Our empirical goals are therefore to verify: i) the theoretical value T_{base} predicts the empirical $\text{TPV}_{\text{label}}$ computed using Eq. 2; ii) empirical TPV computed on the training and test sets are close (TPV stability); iii) and most importantly, lower TPV correlates with lower clean test error. We examine how these quantities vary as we change architectural width, which in our setups acts as a knob that alters the conditioning of the Jacobian and thereby the geometric regime that SGD selects.

Synthetic Data. Clean inputs are drawn i.i.d. from $\mathcal{N}(0, I)$ and targets follow a linear teacher $y = x^\top w_{\text{true}}$. Noisy targets are obtained by adding Gaussian noise with standard deviation $\sigma = 0.01$. We train MLPs with widths $\{128, 256, 512, 800, 1024, 1600\}$. Full details appear in Appendix F.2.1. Figure 5 and Figure 14 (Appendix) summarize the results.

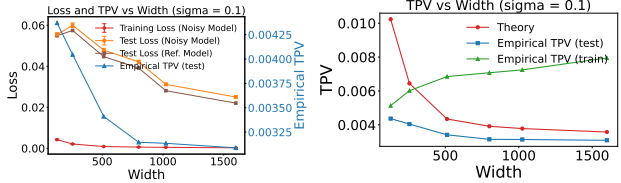


Figure 7. Empirical and theoretical TPV estimates under label noise on synthetic data for noise standard deviation $\sigma = 0.1$. As width increases, theoretical TPV and empirical test set TPV reduce, but training set TPV increases, breaking TPV stability when σ is large.

Across widths, we observe a consistent pattern: as models achieve lower test loss, the corresponding empirical TPV (both training and test versions) and theoretical $\text{TPV}_{\text{label}}$ decrease as well. This confirms that TPV captures the same geometric effects that drive generalization. At small widths, empirical TPV estimates deviate more strongly from the theoretical prediction, whereas at larger widths they closely track $\text{TPV}_{\text{label}}$, consistent with the improved stability of the local linear approximation. Figure 14 (Appendix) confirms that width indeed acts as a knob modulating the conditioning of the Jacobian.

Next, we increase the label-noise standard deviation to $\sigma = 0.1$. This larger noise requires models to move farther from the clean reference solution, violating the first-order approximation underlying Eq. 10. As expected, TPV stability breaks: the training-set empirical TPV approaches σ^2 once the noisy model fits the training data, and the dependence on geometric structure diminishes. However, the *test-set* empirical TPV remains aligned with the theoretical TPV (particularly at larger widths), and continues to correlate with test loss (Figure 7). Thus, even when the first-order assumption is violated, test-set TPV continues to reflect generalization behavior.

CIFAR-10/100 & Imagenet: We perform an analogous experiment on CIFAR-100 using pretrained MobileNetV2 models with varying width multipliers. For each reference model, we treat the predicted logits on the training set as clean regression targets and perturb them with i.i.d. Gaussian noise ($\sigma = 0.1$). We then fine-tune each model on these noisy regression targets and estimate empirical TPV using both the training and test sets, alongside the clean-test cross-entropy of the reference and noisy models. Results are shown in Figure 8.

As the geometric regime changes with width, we again find that models with larger width have lower test loss and exhibit lower empirical TPV, and that training and test TPV estimates are similar in magnitude and trend (TPV stability). CIFAR-10 results and experiment details appear in Appendix F.2.2. A similar experiment on Imagenet where we track empirical TPV along with the validation accuracy

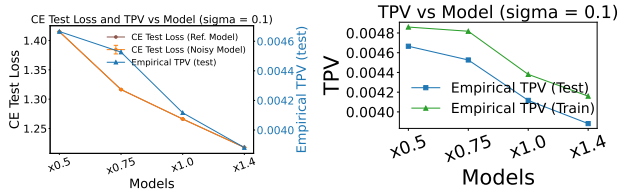


Figure 8. Empirical TPV estimates under label noise on CIFAR-100 for noise standard deviation $\sigma = 0.1$. Both TPV estimates reduce as width increases and correlate with the test set cross-entropy loss of the reference model.

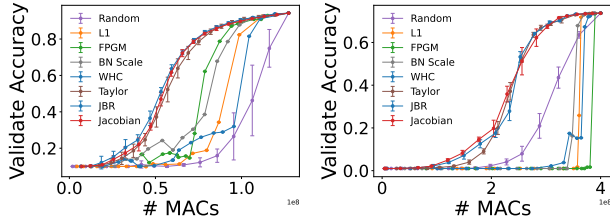


Figure 9. Pruning results of various criteria on Cifar-10 with ResNet-56 (left) and Cifar-100 with VGG-19 (right). JBR matches or outperforms existing methods.

is shown in Fig. 6 (see Appendix F.2.3 for details).

5.3. Pruning

We evaluate whether the TPV-motivated pruning criterion (JBR) improves accuracy–compression tradeoffs relative to standard groupwise criteria. Following the OBC pruning protocol, we perform global channel pruning with iterative removal and recomputation of importance scores. We compare JBR against Jacobian, L1-norm, BatchNorm-scale, FPGM, WHC, Taylor, and Random. We prune two ImageNet models (ResNet-50, MobileNet-V2) at 50% global sparsity and two CIFAR models (ResNet-56 on CIFAR-10, VGG-19-BN on CIFAR-100) at 90% sparsity. Each model is pruned iteratively for 18 steps, averaging results over 5 independent runs. Results are shown in Fig. 9 and Fig. 10 in terms of MACs. Across all architectures, the JBR criterion consistently matches or exceeds the performance of all baselines. See Appendix F.3 for details.

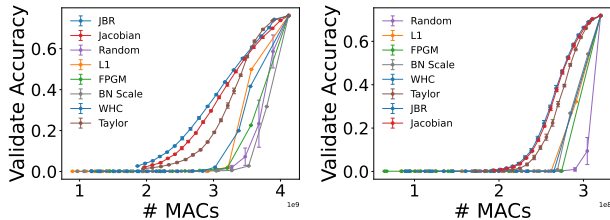


Figure 10. Pruning results of various criteria on ImageNet dataset using ResNet-50 (left) and MobileNet-v2 (right) without fine-tuning. JBR matches or outperforms existing methods.

6. Discussion and conclusion

We introduced TPV as a simple but powerful variance-based framework for probing the robustness of a trained neural network under specific noise sources. We proved that in overparameterized regime, training-set TPV tends to test-set TPV, and empirically showed that this TPV stability holds remarkably well even in extremely narrow networks, as long as a sufficient number of samples is used and the first order approximation holds. This leads us to believe that we may have found a sufficient condition under which TPV stability holds, but it may not be a necessary one.

A key advantage of using TPV over global variance in the global bias-variance decomposition is that TPV studies the properties of a specific trained model rather than all the possible models obtainable by a learning algorithm, which is also what we ultimately care about in real world–robustness of a trained model rather than the properties of the algorithm that trained it. Similar to how modern global bias-variance studies show that bias and variance typically tend to walk hand-in-hand in modern deep networks, we find that TPV estimates tend to correlate with standard test set loss across real world datasets and architectures.

TPV can be used to measure the robustness of a trained model w.r.t. specific perturbation sources and therefore acts as a surgical tool to study generalization at a fine-grained level. In this paper, we showed that studying TPV for both SGD noise (Theorem 3.3) and quantization noise (Remark 3.4) leads to the wide minima hypothesis. This hypothesis is widely used as a tool for model selection and even guiding optimization (Foret et al., 2020). Under the TPV framework, we see that this hypothesis probes the robustness of a model under a specific class of parameter perturbations. Modeling label noise as a source of perturbation under the TPV framework leads to a different TPV estimate (Theorem 3.2) that depends on the spectrum of the output-parameter Jacobian and its alignment between training and test data distributions, and revealed a different practical approach to measuring TPV. We empirically found this object to also correlate with the standard test set loss for various datasets and models. One can similarly probe TPV under perturbations induced by a different noise source.

We believe TPV framework can serve as a foundation for future work on: (i) a deep empirical analysis that compares and contrasts a single model’s robustness w.r.t. different noise sources using the TPV framework; (ii) formalizing new noise sources other than the ones studied in this work (label noise, SGD noise, etc.); for instance, input perturbations (adversarial or domain shift); (iii) improving the algorithm for empirically estimating label noise TPV (see Appendix C.3); (iv) extending the TPV stability analysis to finite-width networks and TPV derivations to loss functions other than MSE.

References

- Adlam, B. and Pennington, J. The neural tangent kernel in high dimensions: Triple descent and a multi-scale theory of generalization. In *International Conference on Machine Learning*, pp. 74–84. PMLR, 2020a.
- Adlam, B. and Pennington, J. Understanding double descent requires a fine-grained bias-variance decomposition. *Advances in neural information processing systems*, 33: 11022–11032, 2020b.
- Allen-Zhu, Z., Li, Y., and Song, Z. A convergence theory for deep learning via over-parameterization. In *Proceedings of the 36th International Conference on Machine Learning (ICML)*, volume 97 of *Proceedings of Machine Learning Research*, pp. 242–252. PMLR, 2019. URL <http://proceedings.mlr.press/v97/allen-zhu19a/allen-zhu19a.pdf>.
- Arora, S., Du, S. S., Hu, W., Li, Z., Salakhutdinov, R. R., and Wang, R. On exact computation with an infinitely wide neural net. *Advances in neural information processing systems*, 32, 2019.
- Bar, A., Mulayoff, R., Michaeli, T., and Talmon, R. The expected loss of preconditioned langevin dynamics reveals the hessian rank. In *Proceedings of the AAAI Conference on Artificial Intelligence*, 2024.
- Barshan, E., Brunet, M.-A., and Dziugaite, G. K. A connection between the fisher information and the hessian of the loss. In *Proceedings of the 23rd International Conference on Artificial Intelligence and Statistics*, volume 108 of *Proceedings of Machine Learning Research*, pp. 1–9, 2020.
- Bartlett, P. L., Tsigler, A., et al. Benign overfitting in linear regression. *Proceedings of the National Academy of Sciences*, 117(48):30063–30070, 2020. doi: 10.1073/pnas.1907378117. Preprint arXiv:1906.11300 (2019).
- Belkin, M., Hsu, D., Ma, S., and Mandal, S. Reconciling modern machine-learning practice and the classical bias-variance trade-off. *PNAS*, 2019.
- Belkin, M., Hsu, D., and Xu, J. Two models of double descent for weak features. *SIAM Journal on Mathematics of Data Science*, 2(4):1167–1180, 2020.
- Bombari, S., Amani, M. H., and Mondelli, M. Memorization and optimization in deep neural networks with minimum over-parameterization. *Advances in Neural Information Processing Systems*, 35:7628–7640, 2022.
- Bordelon, B. and Pehlevan, C. Dynamics of finite width kernel and prediction fluctuations in mean field neural networks. *Advances in Neural Information Processing Systems*, 36:9707–9750, 2023.
- Chaudhari, P. and Soatto, S. Stochastic gradient descent performs variational inference, converges to limit cycles, and generalizes. In *ICLR*, 2018.
- Chen, S., Sun, W., and Huang, L. Whc: Weighted hybrid criterion for filter pruning on convolutional neural networks. In *ICASSP 2023-2023 IEEE International Conference on Acoustics, Speech and Signal Processing (ICASSP)*, pp. 1–5. IEEE, 2023.
- Chen, S., Ma, W., Huang, B., Wang, Q., Wang, G., Sun, W., Huang, L., and John, D. Optimal brain connection: Towards efficient structural pruning. *arXiv preprint arXiv:2508.05521*, 2025.
- Dinh, L., Pascanu, R., Bengio, S., and Bengio, Y. Sharp minima can generalize for deep nets. In *International Conference on Machine Learning*, pp. 1019–1028. PMLR, 2017.
- Du, S. S., Zhai, X., Póczos, B., and Singh, A. Gradient descent provably optimizes over-parameterized neural networks. *arXiv preprint arXiv:1810.02054*, 2018.
- Foret, P., Kleiner, A., Mobahi, H., and Neyshabur, B. Sharpness-aware minimization for efficiently improving generalization. *arXiv preprint arXiv:2010.01412*, 2020.
- Frankle, J. and Carbin, M. The lottery ticket hypothesis: Finding sparse, trainable neural networks. *arXiv preprint arXiv:1803.03635*, 2018.
- Friedman, J. H. On bias, variance, 0/1 loss, and the curse of dimensionality. Technical Report CSD-TR-1997-1027, Department of Statistics, Stanford University, 1997.
- Geman, S., Bienenstock, E., and Doursat, R. Neural networks and the bias/variance dilemma. *Neural Computation*, 4(1):1–58, 1992.
- Han, S., Pool, J., Tran, J., and Dally, W. Learning both weights and connections for efficient neural network. *Advances in neural information processing systems*, 28, 2015.
- Hassibi, B., Stork, D. G., and Wolff, G. J. Optimal brain surgeon and general network pruning. In *IEEE international conference on neural networks*, pp. 293–299. IEEE, 1993.
- He, Y., Liu, P., Wang, Z., Hu, Z., and Yang, Y. Filter pruning via geometric median for deep convolutional neural networks acceleration. In *Proceedings of the IEEE/CVF conference on computer vision and pattern recognition*, pp. 4340–4349, 2019.
- Hochreiter, S. and Schmidhuber, J. Flat minima. *Neural computation*, 9(1):1–42, 1997.

- Jacot, A., Gabriel, F., and Hongler, C. Neural tangent kernel: Convergence and generalization in neural networks. *Advances in neural information processing systems*, 31, 2018.
- Jastrzebski, S., Kenton, Z., Arpit, D., Ballas, N., Fischer, A., Bengio, Y., and Storkey, A. Three factors influencing minima in sgd. *arXiv preprint arXiv:1711.04623*, 2017.
- Keskar, N. S. and et al. On large-batch training for deep learning: Generalization gap and sharp minima. In *ICLR*, 2017.
- Kühn, M. and Rosenow, B. Correlated noise in epoch-based stochastic gradient descent: Implications for weight variances. *arXiv preprint arXiv:2306.05300*, 2023.
- LeCun, Y., Denker, J., and Solla, S. Optimal brain damage. *Advances in neural information processing systems*, 2, 1989.
- Lee, J., Xiao, L., Schoenholz, S., Bahri, Y., Novak, R., Sohl-Dickstein, J., and Pennington, J. Wide neural networks of any depth evolve as linear models under gradient descent. *Advances in neural information processing systems*, 32, 2019.
- Li, H., Kadav, A., Durdanovic, I., Samet, H., and Graf, H. P. Pruning filters for efficient convnets. In *International Conference on Learning Representations (ICLR)*, 2017. Poster.
- Liu, L., Zhang, S., Kuang, Z., Zhou, A., Xue, J.-H., Wang, X., Chen, Y., Yang, W., Liao, Q., and Zhang, W. Group fisher pruning for practical network compression. In *International Conference on Machine Learning*, pp. 7021–7032. PMLR, 2021.
- Liu, Z., Li, J., Shen, Z., Huang, G., Yan, S., and Zhang, C. Learning efficient convolutional networks through network slimming. In *Proceedings of the IEEE international conference on computer vision*, pp. 2736–2744, 2017.
- Mandt, S., Hoffman, M. D., and Blei, D. M. A variational analysis of stochastic gradient algorithms. In *Proceedings of the 33rd International Conference on Machine Learning*, volume 48 of *Proceedings of Machine Learning Research*, pp. 354–363, 2016.
- Mandt, S., Hoffman, M. D., and Blei, D. M. Stochastic gradient descent as approximate bayesian inference. *Journal of Machine Learning Research*, 18(134):1–35, 2017.
- Molchanov, P., Tyree, S., Karras, T., Aila, T., and Kautz, J. Pruning convolutional neural networks for resource efficient inference. *arXiv preprint arXiv:1611.06440*, 2016.
- Molchanov, P., Mallya, A., Tyree, S., Frosio, I., and Kautz, J. Importance estimation for neural network pruning. In *Proceedings of the IEEE/CVF conference on computer vision and pattern recognition*, pp. 11264–11272, 2019.
- Mori, T. Power-law escape rate of stochastic gradient descent. In *Proceedings of the 39th International Conference on Machine Learning*, volume 162 of *Proceedings of Machine Learning Research*, pp. 15928–15966, 2022.
- Neal, B., Mittal, S., Baratin, A., Tantia, V., Scicluna, M., Lacoste-Julien, S., and Mitliagkas, I. A modern take on the bias–variance tradeoff in neural networks. *arXiv preprint arXiv:1810.08591*, 2018.
- Paul, M., Chen, F., Larsen, B. W., Frankle, J., Ganguli, S., and Dziugaite, G. K. Unmasking the lottery ticket hypothesis: What’s encoded in a winning ticket’s mask? *arXiv preprint arXiv:2210.03044*, 2022.
- Rahaman, N., Baratin, A., Arpit, D., Draxler, F., Lin, M., Hamprecht, F., Bengio, Y., and Courville, A. On the spectral bias of neural networks. In *International conference on machine learning*, pp. 5301–5310. PMLR, 2019.
- Singh, P., Verma, V. K., Rai, P., and Nambodiri, V. Leveraging filter correlations for deep model compression. In *Proceedings of the IEEE/CVF Winter Conference on applications of computer vision*, pp. 835–844, 2020.
- Smith, S. L. and Le, Q. V. A bayesian perspective on generalization and stochastic gradient descent. *ICLR*, 2018.
- Soudry, D., Hoffer, E., Nacson, M. S., Gunasekar, S., and Srebro, N. The implicit bias of gradient descent on separable data. *Journal of Machine Learning Research*, 19 (70):1–57, 2018.
- Theis, L., Korshunova, I., Tejani, A., and Huszár, F. Faster gaze prediction with dense networks and fisher pruning. *arXiv preprint arXiv:1801.05787*, 2018.
- Thomas, V., Pedregosa, F., Merriënboer, B., Manzagol, P.-A., Bengio, Y., and Le Roux, N. On the interplay between noise and curvature and its effect on optimization and generalization. In *International Conference on Artificial Intelligence and Statistics*, pp. 3503–3513. PMLR, 2020.
- Wang, C., Zhang, G., and Grosse, R. Picking winning tickets before training by preserving gradient flow. *arXiv preprint arXiv:2002.07376*, 2020.
- Wu, L., Wang, M., and Su, W. The alignment property of sgd noise and how it helps select flat minima. In *Advances in Neural Information Processing Systems*, 2022.

- Xu, Z.-Q. J., Zhang, Y., Luo, T., Xiao, Y., and Ma, Z. Frequency principle: Fourier analysis sheds light on deep neural networks. *arXiv preprint arXiv:1901.06523*, 2019.
- Yang, Z., Yu, Y., You, C., Steinhardt, J., and Ma, Y. Rethinking bias-variance trade-off for generalization of neural networks. In *International Conference on Machine Learning*, pp. 10767–10777. PMLR, 2020.
- You, Z., Yan, K., Ye, J., Ma, M., and Wang, P. Gate decorator: Global filter pruning method for accelerating deep convolutional neural networks. *Advances in neural information processing systems*, 32, 2019.
- Zhang, C., Bengio, S., Hardt, M., Recht, B., and Vinyals, O. Understanding deep learning requires rethinking generalization. In *ICLR*, 2017.
- Zhu, Z., Wu, J., Yu, B., Wu, L., and Ma, J. The anisotropic noise in stochastic gradient descent: Its behavior of escaping from sharp minima and regularization effects. *arXiv preprint arXiv:1803.00195*, 2018.

A. TPV Trace Stability via NTK Stability and LLN

We provide a finite-sample version of the TPV trace stability result used in the main text. Let

$$X_{\text{tr}} = \{x_i\}_{i=1}^{n_{\text{tr}}}, \quad X_{\text{te}} = \{x'_j\}_{j=1}^{n_{\text{te}}}$$

denote the training and test sets, respectively, with both drawn i.i.d. from the same data distribution \mathcal{D} independently of the network initialization.

For any dataset X of size n_X , let $J_X(w) \in \mathbb{R}^{n_X \times p}$ be the Jacobian of network outputs with respect to parameters w . Following the main text, we define

$$H_{\text{eff}}(w; X) = \frac{1}{n_X} J_X(w)^\top J_X(w), \quad (18)$$

and the corresponding empirical NTK Gram matrix

$$G_X(w) = \frac{1}{n_X} J_X(w) J_X(w)^\top. \quad (19)$$

Note that the nonzero eigenvalues of $H_{\text{eff}}(w; X)$ and $G_X(w)$ are identical for every w .

The TPV trace on X is

$$\text{TPV}(w; X) = \text{Tr}(H_{\text{eff}}(w; X) C), \quad (20)$$

where $C \succeq 0$ is the parameter-perturbation covariance.

A.1. Assumptions

We make the following standard assumptions.

Assumption A.1 (i.i.d. train/test). X_{tr} and X_{te} are drawn i.i.d. from the same distribution \mathcal{D} , independently of w_0 .

Assumption A.2 (Finite-set NTK stability). Let w_t be the parameter vector after t steps of gradient descent on X_{tr} , and let $w^* := w_T$ be the trained network. In the infinite-width NTK regime ($m \rightarrow \infty$), individually for the fixed finite datasets $X \in \{X_{\text{tr}}, X_{\text{te}}\}$,

$$\|G_X(w^*) - G_X(w_0)\|_{\text{op}} \leq \varepsilon_{\text{NTK}}, \quad (21)$$

with probability $\rightarrow 1$ as $m \rightarrow \infty$.

Since $H_{\text{eff}}(w; X)$ and $G_X(w)$ share their nonzero spectrum, Assumption A.2 implies

$$\|H_{\text{eff}}(w^*; X) - H_{\text{eff}}(w_0; X)\|_{\text{op}} \leq \varepsilon_{\text{NTK}}. \quad (22)$$

We assume $\|C\|_F < \infty$, which holds for any fixed finite covariance.

A.2. Initialization Consistency via LLN

Define the per-example H_{eff} contribution

$$h(x; w_0) := J(x; w_0)^\top J(x; w_0),$$

so that

$$H_{\text{eff}}(w_0; X) = \frac{1}{n_X} \sum_{x \in X} h(x; w_0).$$

Lemma A.3 (LLN at initialization). Let $\bar{H}_{\text{eff}}(w_0) := \mathbb{E}_{x \sim \mathcal{D}}[h(x; w_0)]$. If $\mathbb{E}\|J(x; w_0)\|_F^2 < \infty$ (i.e., well behaved output-parameter Jacobian), then under Assumption A.1,

$$\|H_{\text{eff}}(w_0; X_{\text{tr}}) - H_{\text{eff}}(w_0; X_{\text{te}})\|_{\text{op}} = o_{n_{\text{tr}}, n_{\text{te}}}(1), \quad (23)$$

where $o_{n_{\text{tr}}, n_{\text{te}}}(1)$ converges to 0 almost surely as $n_{\text{tr}}, n_{\text{te}} \rightarrow \infty$.

Proof. Since $h(x; w_0) := J(x; w_0)^\top J(x; w_0)$ is integrable in Frobenius norm ($\mathbb{E}\|h(x; w_0)\|_F < \infty$) and takes values in the finite-dimensional normed space $(\mathbb{R}^{p \times p}, \|\cdot\|_F)$, applying the strong law of large numbers (LLN) individually to $X \in \{X_{\text{tr}}, X_{\text{te}}\}$, we obtain:

$$\frac{1}{n_X} \sum_{i=1}^{n_X} h(x_i; w_0) \xrightarrow[n_X \rightarrow \infty]{\text{a.s.}} \mathbb{E}_{x \sim \mathcal{D}}[h(x; w_0)] = \bar{H}_{\text{eff}}(w_0),$$

in Frobenius norm. Using $\|\cdot\|_{\text{op}} \leq \|\cdot\|_F$, we also have

$$\|H_{\text{eff}}(w_0; X) - \bar{H}_{\text{eff}}(w_0)\|_{\text{op}} \xrightarrow[n_X \rightarrow \infty]{\text{a.s.}} 0,$$

To obtain the difference bound (23), we use the triangle inequality in operator norm:

$$\begin{aligned} \|H_{\text{eff}}(w_0; X_{\text{tr}}) - H_{\text{eff}}(w_0; X_{\text{te}})\|_{\text{op}} &\leq \|H_{\text{eff}}(w_0; X_{\text{tr}}) - \bar{H}_{\text{eff}}(w_0)\|_{\text{op}} \\ &\quad + \|\bar{H}_{\text{eff}}(w_0) - H_{\text{eff}}(w_0; X_{\text{te}})\|_{\text{op}}. \end{aligned}$$

Each term on the right-hand side converges almost surely to 0 by the LLN argument above, so the sum converges to 0 almost surely as $n_{\text{tr}}, n_{\text{te}} \rightarrow \infty$. \square

A.3. Main Result

Theorem A.4 (TPV trace stability on finite train/test split). *Under Assumptions A.1 and A.2, and $C \succeq 0$, for the trained parameter w^* ,*

$$|\text{TPV}(w^*; X_{\text{tr}}) - \text{TPV}(w^*; X_{\text{te}})| \leq (2\varepsilon_{\text{NTK}} + o_{n_{\text{tr}}, n_{\text{te}}}(1)) \text{Tr}(C).$$

where $\varepsilon_{\text{NTK}} \rightarrow 0$ as $m \rightarrow \infty$ and $o_{n_{\text{tr}}, n_{\text{te}}}(1) \rightarrow 0$ as $n_{\text{tr}}, n_{\text{te}} \rightarrow \infty$.

Proof. Using (20) and symmetry of H_{eff} and C ,

$$|\text{TPV}(w^*; X_{\text{tr}}) - \text{TPV}(w^*; X_{\text{te}})| = |\text{Tr}([H_{\text{eff}}(w^*; X_{\text{tr}}) - H_{\text{eff}}(w^*; X_{\text{te}})] C)|.$$

Now applying the following inequality for a PSD matrix B and an arbitrary symmetric matrix A ,

$$|\text{Tr}(AB)| \leq \|A\|_{\text{op}} \text{Tr}(B),$$

gives

$$|\text{TPV}(w^*; X_{\text{tr}}) - \text{TPV}(w^*; X_{\text{te}})| \leq \text{Tr}(C) \|H_{\text{eff}}(w^*; X_{\text{tr}}) - H_{\text{eff}}(w^*; X_{\text{te}})\|_{\text{op}}.$$

Using the triangle inequality and the operator-norm stability (22),

$$\begin{aligned} &\|H_{\text{eff}}(w^*; X_{\text{tr}}) - H_{\text{eff}}(w^*; X_{\text{te}})\|_{\text{op}} \\ &\leq \|H_{\text{eff}}(w^*; X_{\text{tr}}) - H_{\text{eff}}(w_0; X_{\text{tr}})\|_{\text{op}} + \|H_{\text{eff}}(w_0; X_{\text{tr}}) - H_{\text{eff}}(w_0; X_{\text{te}})\|_{\text{op}} \\ &\quad + \|H_{\text{eff}}(w_0; X_{\text{te}}) - H_{\text{eff}}(w^*; X_{\text{te}})\|_{\text{op}} \\ &\leq 2\varepsilon_{\text{NTK}} + o_{n_{\text{tr}}, n_{\text{te}}}(1), \end{aligned}$$

where the $o_{n_{\text{tr}}, n_{\text{te}}}(1)$ term is from (23). Thus,

$$|\text{TPV}(w^*; X_{\text{tr}}) - \text{TPV}(w^*; X_{\text{te}})| \leq (2\varepsilon_{\text{NTK}} + o_{n_{\text{tr}}, n_{\text{te}}}(1)) \text{Tr}(C).$$

\square

B. TPV for Linear Regression under Label Noise: Benign Overfitting

From $y = X\theta^* + \varepsilon$ and the definition of w^* ,

$$w^* = X^\top (XX^\top)^{-1} (X\theta^* + \varepsilon) = \theta^* + X^\top (XX^\top)^{-1} \varepsilon,$$

using the assumption that θ^* lies in the row span of X . Hence

$$\delta w := w^* - \theta^* = X^\top (XX^\top)^{-1} \varepsilon,$$

so the parameter covariance is

$$C = \text{Cov}(\delta w) = \sigma^2 X^\top (XX^\top)^{-2} X.$$

By whitened input distribution assumption, $H_{\text{eff}} = \mathbb{E}_x [xx^\top] = I_d$, so

$$\text{Tr}(H_{\text{eff}}C) = \text{Tr}(C) = \sigma^2 \text{Tr}(X^\top (XX^\top)^{-2} X).$$

Using the cyclic property of trace, $\text{Tr}(X^\top (XX^\top)^{-2} X) = \text{Tr}((XX^\top)^{-1})$, yielding

$$\text{Tr}(H_{\text{eff}}C) = \sigma^2 \text{Tr}((XX^\top)^{-1}),$$

which matches the classical expression for the expected test prediction variance in overparameterized linear regression.

C. TPV for Non-Linear Regression Under Label Noise

C.1. Proof

We consider a scalar-output model $f_w : \mathbb{R}^d \rightarrow \mathbb{R}$ with parameters $w \in \mathbb{R}^p$, trained on a dataset $\{(x_i, y_i)\}_{i=1}^n$, where $y_i = f_{\theta^*}(x_i)$ (without noise) for some fixed function f_{θ^*} . Let w^* denote a parameter vector that satisfies $f_{w^*}(x_i) = f_{\theta^*}(x_i)$ for all training inputs.

We now perturb the training labels by additive noise:

$$y' = y + \varepsilon,$$

where $y = (y_1, \dots, y_n)^\top \in \mathbb{R}^n$ is the original label vector and $\varepsilon \in \mathbb{R}^n$ is the label perturbation (noise).

We are interested in the stationary points $w^* + \delta w$ of the squared loss with respect to the perturbed labels y' under the first order Taylor's expansion around w^* . Under this approximation, the loss for $w^* + \delta w$ and labels $y' = y + \varepsilon$ is approximated by

$$L(\delta w; y') := \frac{1}{2} \|f(w^*) + J\delta w - (y + \varepsilon)\|^2. \quad (24)$$

where,

$$f(w) := \begin{bmatrix} f_w(x_1) \\ \vdots \\ f_w(x_n) \end{bmatrix} \in \mathbb{R}^n,$$

and similarly defining the Jacobian of the training outputs w.r.t. parameters at w^* ,

$$J := \begin{bmatrix} g(x_1)^\top \\ \vdots \\ g(x_n)^\top \end{bmatrix} \in \mathbb{R}^{n \times p}, \quad (25)$$

Assuming that w^* already fits the original labels well, so that $f(w^*) = y$, we approximate

$$f(w^*) + J\delta w - (y + \varepsilon) = J\delta w - \varepsilon,$$

and hence

$$L(\delta w; y') = \frac{1}{2} \|J\delta w - \varepsilon\|^2. \quad (26)$$

Thus, in the linearized regime, the effect of label noise is captured by the least-squares problem

$$\min_{\delta w \in \mathbb{R}^p} \frac{1}{2} \|J\delta w - \varepsilon\|^2. \quad (27)$$

The gradient of $L(\delta w; y')$ with respect to δw is

$$\nabla_{\delta w} L(\delta w; y') = J^\top (J\delta w - \varepsilon).$$

Setting this to zero yields the *normal equations*

$$J^\top J\delta w = J^\top \varepsilon. \quad (28)$$

Recall that we are interested in finding the min-norm solution among all the δw that satisfy the above equation, i.e. $\arg \min_{\delta w} \{\|\delta w\|^2 \text{ s.t. } \nabla_{\delta w} L(\delta w; y') = 0\}$. To analytically find this min-norm solution, we start with the compact SVD of J :

$$J = U_r S V_r^\top, \quad (29)$$

where

- $U_r \in \mathbb{R}^{n \times r}$ with orthonormal columns ($U_r^\top U_r = I_r$),
- $V_r \in \mathbb{R}^{p \times r}$ with orthonormal columns ($V_r^\top V_r = I_r$),
- $S \in \mathbb{R}^{r \times r}$ is diagonal with positive singular values $S = \text{diag}(s_1, \dots, s_r)$, where $s_i > 0$.

Substituting (29) into (28), we have

$$J^\top J\delta w = V_r S U_r^\top U_r S V_r^\top \delta w = V_r S^2 V_r^\top \delta w$$

and

$$J^\top \varepsilon = (U_r S V_r^\top)^\top \varepsilon = V_r S U_r^\top \varepsilon.$$

Thus the normal equations become

$$V_r S^2 V_r^\top \delta w = V_r S U_r^\top \varepsilon. \quad (30)$$

Left-multiplying by V_r^\top and defining $\alpha := V_r^\top \delta w \in \mathbb{R}^r$, we obtain

$$S^2 \alpha = S U_r^\top \varepsilon \quad \Rightarrow \quad S \alpha = U_r^\top \varepsilon \quad \Rightarrow \quad \alpha = S^{-1} U_r^\top \varepsilon.$$

Any δw can be decomposed into components along the range of V_r and its orthogonal complement. Extending V_r to an orthonormal basis $[V_r \ V_\perp] \in \mathbb{R}^{p \times p}$, we can write

$$\delta w = V_r \alpha + V_\perp \beta,$$

for some $\beta \in \mathbb{R}^{p-r}$. The normal equations constrain only the component along V_r , giving $\alpha = S^{-1} U_r^\top \varepsilon$, while β is unconstrained (it lies in the nullspace of J).

The *minimum-norm* solution is obtained by setting $\beta = 0$, yielding

$$\delta w_{\min} = V_r S^{-1} U_r^\top \varepsilon. \quad (31)$$

For a new test input x , the first-order Taylor expansion gives

$$f_{w^* + \delta w}(x) \approx f_{w^*}(x) + g(x)^\top \delta w, \quad (32)$$

where $g(x) = \nabla_w f_{w^*}(x)$. Note that this is the gradient of the output, not the loss. Hence the prediction change is

$$\delta f(x) := f_{w^* + \delta w}(x) - f_{w^*}(x) \approx g(x)^\top \delta w. \quad (33)$$

Plugging in the minimum-norm solution (31), we get

$$\delta f(x) \approx g(x)^\top V_r S^{-1} U_r^\top \varepsilon. \quad (34)$$

We now decompose the test gradient $g(x)$ in the parameter-space basis $[V_r \ V_\perp]$:

$$g(x) = V_r b(x) + V_\perp c(x),$$

where

$$b(x) := V_r^\top g(x) \in \mathbb{R}^r, \quad c(x) := V_\perp^\top g(x) \in \mathbb{R}^{p-r}.$$

Using orthogonality $V_r^\top V_\perp = 0$, we have

$$g(x)^\top V_r S^{-1} U_r^\top \varepsilon = b(x)^\top S^{-1} U_r^\top \varepsilon.$$

Thus the prediction change for the minimum-norm solution is

$$\delta f(x) = b(x)^\top S^{-1} U_r^\top \varepsilon, \quad b(x) = V_r^\top g(x). \quad (35)$$

We now treat the label noise as random from any distribution such that it has zero mean and covariance $\mathbb{E}[\varepsilon \varepsilon^\top] = \sigma_\varepsilon^2 I_n$.

Define

$$\eta := U_r^\top \varepsilon \in \mathbb{R}^r.$$

Since U_r has orthonormal columns and ε is isotropic, we have

$$\mathbb{E}[\eta] = 0, \quad \mathbb{E}[\eta \eta^\top] = \sigma_\varepsilon^2 I_r.$$

Using (35), we can rewrite

$$\delta f(x) = b(x)^\top S^{-1} \eta.$$

For a fixed test input x , the mean and variance over label noise are:

Mean.

$$\mathbb{E}_\varepsilon[\delta f(x)] = b(x)^\top S^{-1} \mathbb{E}[\eta] = 0.$$

Variance.

$$\begin{aligned} \mathbb{E}_\varepsilon [(\delta f(x))^2] &= \mathbb{E}_\varepsilon [b(x)^\top S^{-1} \eta \eta^\top S^{-1} b(x)] \\ &= b(x)^\top S^{-1} \mathbb{E}_\varepsilon [\eta \eta^\top] S^{-1} b(x) \\ &= \sigma_\varepsilon^2 b(x)^\top S^{-2} b(x), \end{aligned} \quad (36)$$

where $S^{-2} = S^{-1} S^{-1} = \text{diag}(1/s_1^2, \dots, 1/s_r^2)$.

To obtain the *expected test prediction variance*, we now average (36) over the test input distribution $x \sim P_X$. Define the second-moment matrix of the projected test gradients:

$$B := \mathbb{E}_{x \sim P_X} [b(x) b(x)^\top] \in \mathbb{R}^{r \times r}. \quad (37)$$

Then

$$\begin{aligned} \mathbb{E}_{x, \varepsilon} [(\delta f(x))^2] &= \mathbb{E}_x [\mathbb{E}_\varepsilon [(\delta f(x))^2 \mid x]] \\ &= \mathbb{E}_x [\sigma_\varepsilon^2 b(x)^\top S^{-2} b(x)] \\ &= \sigma_\varepsilon^2 \mathbb{E}_x [\text{Tr}(S^{-2} b(x) b(x)^\top)] \\ &= \sigma_\varepsilon^2 \text{Tr}(S^{-2} \mathbb{E}_x [b(x) b(x)^\top]) \\ &= \sigma_\varepsilon^2 \text{Tr}(S^{-2} B). \end{aligned} \quad (38)$$

Since S^{-2} is diagonal, we can write this explicitly as

$$\mathbb{E}_{x, \varepsilon} [(\delta f(x))^2] = \sigma_\varepsilon^2 \sum_{i=1}^r \frac{B_{ii}}{s_i^2}, \quad (39)$$

where $B_{ii} = \mathbb{E}_x [b_i(x)^2]$ is the expected squared projection of the Jacobian under the *test data distribution* onto the i -th right singular vector of the training dataset's *empirical Jacobian* J .

C.2. Useful Regime and Pathological Case Analysis

In this section we resolve two subtle but important conceptual points regarding: i) the regime in which the label-noise TPV (Theorem 3.2) is useful; ii) pathological cases where the label-noise TPV object are seemingly different for the training and test sets and TPV stability appears to breaks.

If a model is sufficiently expressive, then it can interpolate arbitrarily small perturbations to the logits on the training set. If interpolation occurs, then we have $f_{w^*+\delta w}(x) - f_{w^*}(x) = \varepsilon$ on the training set and the training-set TPV (Eq. 2) becomes exactly σ_ε^2 for *every* such model.

If now, the test-set TPV from Theorem 3.2 still depends on the Jacobian spectrum and therefore varies across architectures, it may raise the concern that TPV stability has failed. We show below that this is not the case: the interpolation scenario is a special, degenerate limit that violates the assumptions of Theorem 3.2, and is in fact incompatible. If on the other hand, the training and test distributions are identical, then test-set TPV becomes identical to the training set TPV (σ_ε^2). In this case, TPV stability holds trivially, but the label noise TPV object itself loses its discriminative power and is no longer informative.

To shed light on the above concerns, we begin by noting that **Theorem 3.2 does *not* assume interpolation of noisy labels**. Theorem 3.2 analyzes the *local* linearized problem around the clean minimizer w^* . Let $J \in \mathbb{R}^{n \times p}$ be the Jacobian of network outputs at the training inputs. Under label noise ε , the linearized loss is

$$L(\delta w) = \frac{1}{2} \|J\delta w - \varepsilon\|^2,$$

and we find the *minimum-norm* stationary point δw_{\min} satisfying the normal equations $J^\top(J\delta w_{\min} - \varepsilon) = 0$. The solution is

$$\delta w_{\min} = V_r S^{-1} U_r^\top \varepsilon,$$

using the compact SVD $J = U_r S V_r^\top$ with rank $r \leq n$. Theorem 3.2 itself makes no assumption that $J\delta w_{\min} = \varepsilon$; indeed,

$$J\delta w_{\min} = U_r U_r^\top \varepsilon,$$

which equals ε *only* when $r = n$ (full row rank). Thus, interpolation of noisy labels is a special case and is not used anywhere in the proof of Theorem 3.2.

Training TPV in four local regimes. We now distinguish the four local regimes relevant for interpreting TPV.

(1) Ridge/local regime: Our experimental setup constrains the noisy models to remain close to w^* , through explicit proximity regularization. In the linear approximation, this corresponds to solving the *ridge* problem

$$\min_{\delta w} \frac{1}{2} \|J\delta w - \varepsilon\|^2 + \frac{\lambda}{2} \|\delta w\|_2^2,$$

with $\lambda > 0$. The minimizer satisfies $(J^\top J + \lambda I)\delta w_\lambda = J^\top \varepsilon$, giving

$$J\delta w_\lambda = U_r \text{diag}\left(\frac{s_i^2}{s_i^2 + \lambda}\right) U_r^\top \varepsilon,$$

where s_i are the singular values of J . Hence

$$\text{TPV}_{\text{train}} = \frac{1}{n} \mathbb{E}[\|J\delta w_\lambda\|_2^2] = \sigma_\varepsilon^2 \cdot \frac{1}{n} \sum_{i=1}^r \left(\frac{s_i^2}{s_i^2 + \lambda}\right)^2 < \sigma_\varepsilon^2,$$

with explicit dependence on the Jacobian spectrum. Even when $r = n$ (full row rank), the shrinkage factors $s_i^2/(s_i^2 + \lambda)$ are strictly less than 1, so the noisy labels are *not* interpolated and $\text{TPV}_{\text{train}}$ remains strictly below σ_ε^2 . The test TPV is given by Theorem 3.2 (with S^{-2} replaced by ridge-shrunk directions), and Theorem 2.1 guarantees that train and test TPV remain close in this small-perturbation regime (in theory for extremely wide networks).

(2) Pure least-squares, full-row-rank interpolation (degenerate case): We now consider the case $\lambda = 0$, and the linearized least-squares problem admits an exact interpolating solution, and therefore, $\text{rank}(J) = n$. Two related sub-regimes arise.

(2a) *Finite-variance interpolation*: When $r = n$ and $\lambda = 0$, the minimum-norm solution satisfies $J\delta w_{\min} = \varepsilon$, so the noisy labels are interpolated exactly in the linearized model. Consequently,

$$\text{TPV}_{\text{train}} = \sigma_\varepsilon^2.$$

If the train and test distributions match and the Jacobian moments concentrate, then,

$$B = V^\top H_{\text{eff}}(w^*; X_{\text{te}})V \approx V^\top \left(\frac{1}{n}VS^2V^\top\right)V = \frac{1}{n}S^2,$$

i.e., $B_{ii} \approx s_i^2/n$, and Theorem 3.2 gives

$$\text{TPV}_{\text{test}} \approx \sigma_\varepsilon^2 \frac{r}{n} = \sigma_\varepsilon^2.$$

Thus training and test TPV coincide exactly, and TPV stability holds trivially. However, in this interpolation regime TPV loses all discriminative power across architectures, since its value is the same constant σ_ε^2 for all sufficiently expressive models.

(2b) *Infinitesimal-variance interpolation* ($\sigma_\varepsilon^2 \rightarrow 0$): A more extreme version of the interpolation regime occurs when the variance of the injected logit noise is taken to be arbitrarily small. If σ_ε^2 is sufficiently small, then for any model with $r = n$ the optimization remains in the linear regime and still satisfies $J\delta w_{\min} = \varepsilon$. In this case the covariance of the parameter perturbation, $C = \mathbb{E}[\delta w_{\min} \delta w_{\min}^\top] = \sigma_\varepsilon^2 VS^{-2}V^\top$, shrinks to zero as $\sigma_\varepsilon^2 \rightarrow 0$. Therefore both

$$\text{TPV}_{\text{train}} \rightarrow 0, \quad \text{TPV}_{\text{test}} \rightarrow 0,$$

and once again TPV stability holds trivially. As in sub-regime (2a), TPV becomes *uninformative*: although stability is preserved, TPV provides no basis for discriminating among models, as the entire TPV curve collapses to zero in the limit $\sigma_\varepsilon^2 \rightarrow 0$.

Across both sub-regimes (finite or infinitesimal noise), TPV stability remains intact but TPV becomes a constant across architectures, and thus ceases to encode meaningful geometric or generalization differences.

(3) Low-rank or effectively narrow networks: If $r < n$, then even with $\lambda = 0$, the interpolation residual $\varepsilon_{\text{res}} = (I - U_r U_r^\top)\varepsilon$ is non-zero, and

$$\text{TPV}_{\text{train}} = \sigma_\varepsilon^2 \frac{r}{n} < \sigma_\varepsilon^2.$$

In this regime, both training and test TPV depend on r and the Jacobian alignment encoded in B , and TPV is robustly discriminative across architectures. TPV stability becomes non-trivial follows from Theorem 2.1.

(4) Large-noise, non-local regime (Figure 7): There remains one additional regime, which we empirically probe in Fig. 7: the *large-noise, non-local* regime. For sufficiently large noise variance σ_ε^2 , SGD driven by the noisy logits may move the parameters far away from w^* . In this case: (i) the parameter increment δw is no longer small, (ii) the Jacobian $J(w)$ along the optimization path changes substantially, and (iii) the actual solution reached by SGD is not well-approximated by the *local* min-(ridge)-norm solution of the linearized problem at w^* .

Empirically, in this regime we observe that the training noise is effectively interpolated (the network fits the large noisy perturbations), so the *empirical* training TPV saturates near σ_ε^2 and becomes almost independent of width, while the test TPV still varies with width. At first glance this seems to violate TPV stability. However, this behavior occurs precisely when the assumptions of Theorem 3.2 are violated: the first-order approximation around w^* breaks down and the min-(ridge)-norm linearized dynamics no longer describe the optimization. In other words, the large-noise experiment in Fig. 7 is *intentionally outside* the small-perturbation regime where our theory applies. As a result, the mismatch between empirical train and test TPV in this experiment does not constitute a counterexample to TPV stability; it merely marks the breakdown of the underlying linearization and optimization assumptions.

Summary: The discussion above highlights that TPV stability does *not* fail in either of the interpolation regimes described in (2a)–(2b). When the linearized problem interpolates the noisy labels exactly (either for finite σ_ε^2 or in the limit $\sigma_\varepsilon^2 \rightarrow 0$), both the training and test TPV collapse to the same constant (σ_ε^2) or to zero, respectively. In these limits, Theorem 2.1 is satisfied trivially. What is lost in these regimes is not the validity of TPV stability but the *utility* of TPV as a discriminative signal across architectures—TPV becomes identical for all sufficiently expressive models.

On the other hand, the concern that “expressive models always interpolate the noisy logits, forcing $\text{TPV}_{\text{train}} = \sigma_\varepsilon^2$ while test TPV varies” arises **only** when implicitly combining: (i) full row rank ($r = n$) due to exact interpolation on training set, (ii) zero regularization ($\lambda = 0$), and (iii) **ignoring the breakdown of the first-order approximation at large noise**. Theorem 3.2 assumes min-norm dynamics within the local linear region around w^* . In the regime where these assumptions hold (small perturbations, local solutions, matched train/test distributions), both training and test TPV depend on the Jacobian geometry and TPV stability makes training-set TPV a useful object. Note that if the first order approximation is not violated but the other two conditions are still true, then, if training and test set distributions are identical, test-set TPV **has** to be equal to the training-set TPV because of the mathematical relation shown in the case 2a above. In the extreme large-noise or shifted-distribution regimes (e.g., Fig. 7), the theory is not expected to apply, and empirical violations of TPV stability simply signal the breakdown of these assumptions rather than a flaw in the underlying results.

The practically relevant regime, and the one probed in our experiments, is the nontrivial, small-but-finite perturbation setting where the optimization remains local, the noisy labels are *not* interpolated in the linear approximation. In this regime, TPV retains meaningful dependence on the Jacobian geometry as predicted by Theorem 3.2.

C.3. Practical Computation of the Label–Noise TPV Quantity

C.3.1. IDEALIZED LINEARIZED RESPONSE UNDER LABEL NOISE

The label–noise TPV theorem (Section 3.1) analyzes how *infinitesimal* perturbations to the *training labels* propagate through the optimization dynamics to induce fluctuations in *test predictions*. Let

$$J_{\text{tr}} \in \mathbb{R}^{n_{\text{tr}} \times p} \quad \text{and} \quad J_{\text{te}} \in \mathbb{R}^{n_{\text{te}} \times p}$$

denote the Jacobians of the training and test logits with respect to the model parameters, evaluated at the reference point θ^* .

For a perturbation $\varepsilon \in \mathbb{R}^{n_{\text{tr}}}$ to the training labels, the idealized first–order parameter displacement is the *minimum–norm* solution of

$$\delta w^* = \arg \min_{\delta w \in \mathbb{R}^p} \frac{1}{2} \|J_{\text{tr}} \delta w - \varepsilon\|_2^2, \quad (40)$$

which has the closed–form expression

$$\delta w^* = J_{\text{tr}}^\top (J_{\text{tr}} J_{\text{tr}}^\top)^\dagger \varepsilon.$$

This induces the test–prediction perturbation

$$\delta f_{\text{te}}^* = J_{\text{te}} \delta w^* = J_{\text{te}} J_{\text{tr}}^\top (J_{\text{tr}} J_{\text{tr}}^\top)^\dagger \varepsilon.$$

Hence the label–noise TPV is

$$\text{TPV}_{\text{label}} = \mathbb{E}_\varepsilon \left[\|\delta f_{\text{te}}^*\|_2^2 \right],$$

and therefore depends *jointly* on both the training and test Jacobians. The training Jacobian determines how label noise induces parameter motion, while the test Jacobian determines how that motion affects generalization.

C.3.2. DUAL FORMULATION AND IDEAL NUMERICAL COMPUTATION

Equation (40) admits the well–known dual representation

$$(J_{\text{tr}} J_{\text{tr}}^\top + \lambda I) \alpha = \varepsilon, \quad \delta w^* = J_{\text{tr}}^\top \alpha,$$

where $\lambda \geq 0$ is used for finite–variance perturbations or numerical stability. Thus, computing the exact linearized TPV requires repeatedly solving systems of the form

$$A \alpha = \varepsilon, \quad A := J_{\text{tr}} J_{\text{tr}}^\top + \lambda I. \quad (41)$$

Importantly, iterative solvers such as conjugate gradient (CG) require only matrix–vector products of the form $\alpha \mapsto A\alpha$. These can be implemented via standard Jacobian–vector and vector–Jacobian products in modern autodiff systems without forming the full Jacobian. For smaller networks or modest n_{tr} , CG converges rapidly, enabling exact numerical evaluation of the theoretical TPV.

C.3.3. EMPIRICAL OBSERVATION: DEEP-NETWORK JACOBIANS ARE EXTREMELY ILL-CONDITIONED

While we were able to compute the SVD of the training set and test set Jacobians for the synthetic data experiments in Fig. 5, full SVD is not possible for modern architectures like CIFAR-10 MobileNetV2. So we attempted to compute the linearized label-noise TPV using the above CG formulation. Despite using:

- subsampled training sets ($n_{tr} = 2000-4000$),
- ridge regularization ($\lambda > 0$),
- diagonal preconditioners via Hutchinson estimator,

CG *failed to converge* in essentially all settings. Residuals stagnated or oscillated rather than decreasing, and solutions did not approach the correct linearized displacement even after hundreds of iterations. Rayleigh-quotient diagnostics revealed spectral scales for A spanning 10^6-10^8 , implying condition numbers far beyond the regime in which iterative solvers are computationally viable.

Constructing A explicitly is also infeasible: even with $n_{tr} = 4000$, computing A requires thousands of Jacobian-vector products *per logit*. Thus, for large deep networks, the exact linearized TPV $\varepsilon^\top A^{-1} \varepsilon$ is a well-defined mathematical object but a *numerically intractable one*.

C.3.4. PRACTICAL RESOLUTION: LOCAL SGD WITH PROXIMITY REGULARIZATION

Because direct inversion of $J_{tr} J_{tr}^\top$ was numerically intractable for deep networks, we approximate the idealized TPV dynamics using a *local perturb-and-retrain procedure*:

1. Start from the reference parameters θ^* .
2. Perturb the training labels: $\tilde{y} = y + \varepsilon$.
3. Retrain for a small number of steps using the objective

$$\mathcal{L}_{\text{noisy}}(\theta) + \frac{\gamma}{2} \|w - w^*\|_2^2,$$

which ensures optimization remains in the local neighborhood where the linearized approximation is valid.

4. Evaluate prediction changes on *test data*, implicitly incorporating the test Jacobian J_{te} .
5. Estimate TPV as the empirical variance of the test predictions across multiple independent perturbations.

While it does not yield the *exact* minimum-norm linearized solution, it provides a robust local approximation to the TPV dynamics in regimes where the exact computation is infeasible.

Important Practical Considerations: There are a couple of important practical considerations when using SGD based fine-tuning on noisy target logits for estimating label noise TPV:

1. Models need to be trained in eval mode: we perturb the logits of the clean model’s prediction with Gaussian noise and train a copy of the reference model to fit these new targets, which act as infinitesimal change in targets. To achieve this faithfully, training must be done in eval mode, i.e., modules like batch norm and dropout should not be present. The reason is that if these modules are in training mode, even a zero variance perturbation causes the model to have perturbed targets, which is not our goal.
2. Mini-batch shuffling: All sources of randomness other than label noise should be removed as much as possible to isolate the effect of label noise when measuring TPV (e.g. different mini-batch in each epoch). In practice, we do you mini-batch SGD for noisy label fine-tuning for efficiency and to make the training loss go down in some cases. However, we ensure that the sequence of mini-batch remains the same in each epoch or at the very least across different runs. Even though mini-batch gradient is a sum of the expected gradient plus a noise vector, removing random shuffling in this way ensures that each independent run sees the same sequence of mini-batches.

3. MSE training loss must go down during training. This can be easily overlooked, and if the loss does not go down or diverges, it can easily lead to incorrect TPV estimates. We found this to be especially true in the case of ImageNet experiments, where it was extremely difficult to fit noisy target logits.

D. TPV for SGD Stationary Noise

Setup. Consider a scalar-output model $f(x; w)$ trained on a fixed dataset $\{(x_i, y_i)\}_{i=1}^n$ with squared loss

$$L(w) = \frac{1}{2n} \sum_{i=1}^n \varepsilon_i(w)^2, \quad \varepsilon_i(w) := f(x_i; w) - y_i.$$

Let $J_i(w) := \nabla_w f(x_i; w) \in \mathbb{R}^{1 \times p}$ denote the output-parameter Jacobian row, and let $J(w) \in \mathbb{R}^{n \times p}$ be the matrix stacking these rows. Then the per-sample gradient is

$$g_i(w) := \nabla_w \ell_i(w) = \varepsilon_i(w) J_i(w)^\top.$$

D.1. Relation Between Gradient Covariance Matrix and Hessian near Minima

Note that similar proportionality between SGD gradient covariance and curvature (Hessian / Fisher) has been shown in prior work (Wu et al., 2022; Mori, 2022; Mandt et al., 2016; Kühn & Rosenow, 2023; Barshan et al., 2020), typically under population or online assumptions, specific model classes (linear networks, RFMs) or log-likelihood objectives. Here we make this connection explicit for finite-sample nonlinear squared-loss regression on a fixed dataset with no label noise.

Throughout this derivation we fix a parameter w (later evaluated in a small-loss regime near an attractor w^*) and study the covariance of the stochastic gradients induced by random mini-batching, without assuming any stochasticity in the dataset itself.

Per-sample and mini-batch gradient covariance. Let I be a random index uniformly distributed in $\{1, \dots, n\}$. Then

$$g_I(w) = \varepsilon_I(w) J_I(w)^\top.$$

Define the diagonal matrix

$$A_2(w) := \text{diag}(\varepsilon_1(w)^2, \dots, \varepsilon_n(w)^2),$$

and the full-batch gradient

$$g(w) = \nabla_w L(w) = \frac{1}{n} \sum_{i=1}^n g_i(w) = \frac{1}{n} J(w)^\top \varepsilon(w),$$

where $\varepsilon(w) \in \mathbb{R}^n$ stacks the residuals $\varepsilon_i(w)$.

The per-sample gradient covariance (over the random index I) is

$$\Sigma_{\text{sample}}(w) := \text{Cov}(g_I(w)) = \mathbb{E}[g_I(w)g_I(w)^\top] - g(w)g(w)^\top \quad (42)$$

$$= \frac{1}{n} \sum_{i=1}^n \varepsilon_i(w)^2 J_i(w)^\top J_i(w) - \frac{1}{n^2} \left(\sum_{i=1}^n \varepsilon_i(w) J_i(w)^\top \right) \left(\sum_{j=1}^n \varepsilon_j(w) J_j(w)^\top \right)^\top \quad (43)$$

$$= \frac{1}{n} J(w)^\top A_2(w) J(w) - \frac{1}{n^2} J(w)^\top \varepsilon(w) \varepsilon(w)^\top J(w). \quad (44)$$

Thus we have the exact decomposition

$$\boxed{\Sigma_{\text{sample}}(w) = \frac{1}{n} J(w)^\top A_2(w) J(w) - \frac{1}{n^2} J(w)^\top \varepsilon(w) \varepsilon(w)^\top J(w).} \quad (45)$$

Now consider a mini-batch B of size b , sampled uniformly with replacement, and the corresponding mini-batch gradient

$$g_B(w) := \frac{1}{b} \sum_{i \in B} g_i(w).$$

Conditioned on w , the covariance of $g_B(w)$ is

$$\Sigma_\xi(w) := \text{Cov}(g_B(w) - g(w) \mid w) = \text{Cov}(g_B(w) \mid w) = \frac{1}{b} \Sigma_{\text{sample}}(w).$$

Using (45), we obtain

$$\Sigma_\xi(w) = \frac{1}{bn} J(w)^\top A_2(w) J(w) - \frac{1}{bn^2} J(w)^\top \varepsilon(w) \varepsilon(w)^\top J(w). \quad (46)$$

Approximation 1: dropping the $1/n^2$ term. The second term in (46) carries an explicit factor $1/n^2$ and is the image, under $J(w)^\top(\cdot)J(w)$, of a rank-1 matrix $\varepsilon(w)\varepsilon(w)^\top$. In contrast, the first term scales as $1/n$ and involves a diagonal matrix $A_2(w)$. For large n , it is therefore natural to approximate

$$\Sigma_\xi(w) \approx \frac{1}{bn} J(w)^\top A_2(w) J(w). \quad (47)$$

Approximation2: Trace and residual-variance approximation. We now focus on the trace of the gradient noise covariance. Using cyclicity of the trace,

$$\text{Tr}(\Sigma_\xi(w)) \approx \frac{1}{bn} \text{Tr}(J(w)^\top A_2(w) J(w)) \quad (48)$$

$$= \frac{1}{bn} \text{Tr}(A_2(w) J(w) J(w)^\top) \quad (49)$$

$$= \frac{1}{bn} \sum_{i=1}^n \varepsilon_i(w)^2 (J(w) J(w)^\top)_{ii}. \quad (50)$$

At the late-time SGD equilibrium, we model the residuals as random variables induced by the stationary distribution of w_t and make the following approximation:

- (i) the squared residuals $\varepsilon_i(w)^2$ are approximately i.i.d. across samples, with common variance $\mathbb{E}[\varepsilon_i(w)^2] = \sigma_\varepsilon^2$;
- (ii) the residual magnitudes are approximately independent of the geometry encoded in the diagonal entries $(J(w)J(w)^\top)_{ii}$.

Under these assumptions,

$$\mathbb{E}[\text{Tr}(\Sigma_\xi(w))] \approx \frac{1}{bn} \sum_{i=1}^n \mathbb{E}[\varepsilon_i(w)^2] (J(w)J(w)^\top)_{ii} \quad (51)$$

$$\approx \frac{\sigma_\varepsilon^2}{bn} \sum_{i=1}^n (J(w)J(w)^\top)_{ii} = \frac{\sigma_\varepsilon^2}{bn} \text{Tr}(J(w)J(w)^\top). \quad (52)$$

Define the effective Jacobian curvature

$$H_{\text{eff}}(w) := \frac{1}{n} J(w)^\top J(w), \quad (53)$$

so that $\text{Tr}(J(w)J(w)^\top) = n \text{Tr}(H_{\text{eff}}(w))$. We obtain

$$\mathbb{E}[\text{Tr}(\Sigma_\xi(w))] \approx \frac{\sigma_\varepsilon^2}{b} \text{Tr}(H_{\text{eff}}(w)). \quad (54)$$

Thus, up to a scalar factor determined by the residual variance and the mini-batch size b , the trace of the SGD gradient covariance is proportional to the trace of the effective Jacobian curvature H_{eff} .

D.2. Relation Between H_{eff} And Hessian Near Minima

For the squared loss, the Hessian of $L(w)$ is

$$\nabla_w^2 L(w) = \frac{1}{n} \sum_{i=1}^n (J_i(w)^\top J_i(w) + \varepsilon_i(w) \nabla_w^2 f(x_i; w)) \quad (55)$$

$$= \frac{1}{n} \sum_{i=1}^n \underbrace{J_i(w)^\top J_i(w)}_{H_{\text{eff}}(w)} + R(w), \quad (56)$$

where

$$R(w) := \frac{1}{n} \sum_{i=1}^n \varepsilon_i(w) \nabla_w^2 f(x_i; w)$$

collects the second-derivative terms weighted by residuals. In particular,

$$\nabla_w^2 L(w) = H_{\text{eff}}(w) + R(w). \quad (57)$$

Suppose that w lies in a small-loss regime where $|\varepsilon_i(w)|$ is uniformly small for all i , and that the second derivatives $\nabla_w^2 f(x_i; w)$ are uniformly bounded in operator norm. Then $\|R(w)\|$ is small, and $H_{\text{eff}}(w)$ provides a good approximation to the true Hessian:

$$\|\nabla_w^2 L(w) - H_{\text{eff}}(w)\| = \|R(w)\| \leq \frac{1}{n} \sum_{i=1}^n |\varepsilon_i(w)| \|\nabla_w^2 f(x_i; w)\| \ll \|H_{\text{eff}}(w)\|. \quad (58)$$

Consequently, in the late-time regime where training loss is small on all samples, we have

$$\boxed{H_{\text{eff}}(w) \approx \nabla_w^2 L(w)} \quad (59)$$

D.3. SGD Late Dynamics and Relation Between TPV and Hessian

We consider the late-time dynamics of SGD near an attractor w^* of the training dynamics. Writing deviations $\delta w_t = w_t - w^*$, a single SGD step with learning rate η and mini-batch gradient $g_B(w_t)$ can be written as

$$\delta w_{t+1} = \delta w_t - \eta g_B(w_t). \quad (60)$$

Let $g(w_t) = \nabla L(w_t)$ denote the full-batch gradient of the empirical loss L , and define the mini-batch noise as

$$\xi_t := g_B(w_t) - g(w_t), \quad \mathbb{E}[\xi_t | w_t] = 0. \quad (61)$$

Near w^* we linearize the deterministic drift as

$$g(w_t) \approx \nabla_w^2 L(w) \delta w_t, \quad (62)$$

where $\nabla_w^2 L(w)$ is the Hessian. We now use the result from appendix D.2 stating $H_{\text{eff}} \approx \nabla_w^2 L(w)$. Thus,

$$g_B(w_t) \approx H_{\text{eff}} \delta w_t + \xi_t, \quad (63)$$

With this notation, the linearized SGD dynamics become

$$\delta w_{t+1} = (I - \eta H_{\text{eff}}) \delta w_t - \eta \xi_t = A \delta w_t - \eta \xi_t, \quad A := I - \eta H_{\text{eff}}. \quad (64)$$

Let $C_t = \mathbb{E}[\delta w_t \delta w_t^\top]$ denote the covariance of the parameters at time t , and let $\Sigma_\xi = \text{Cov}(\xi_t)$ denote the covariance of the mini-batch noise at w^* . Using the linear update and the fact that ξ_t is independent of δw_t and has zero mean, we obtain the standard covariance recursion

$$C_{t+1} = A C_t A^\top + \eta^2 \Sigma_\xi. \quad (65)$$

Assuming convergence to a stationary distribution, we set $C_{t+1} = C_t = C_{\text{sgd}}$ and obtain the discrete Lyapunov equation

$$C_{\text{sgd}} = AC_{\text{sgd}}A^\top + \eta^2\Sigma_\xi. \quad (66)$$

Thus,

$$ACA^\top = (I - \eta H_{\text{eff}})C_{\text{sgd}}(I - \eta H_{\text{eff}})^\top \quad (67)$$

$$= C_{\text{sgd}} - \eta(H_{\text{eff}}C_{\text{sgd}} + C_{\text{sgd}}H_{\text{eff}}^\top) + \eta^2 H_{\text{eff}}C_{\text{sgd}}H_{\text{eff}}^\top. \quad (68)$$

Plugging this into Eq. (66) and canceling C_{sgd} on both sides yields

$$0 \approx -\eta(H_{\text{eff}}C_{\text{sgd}} + C_{\text{sgd}}H_{\text{eff}}^\top) + \eta^2 H_{\text{eff}}C_{\text{sgd}}H_{\text{eff}}^\top + \eta^2\Sigma_\xi. \quad (69)$$

Neglecting $O(\eta^2)$ terms in the drift (the $H_{\text{eff}}C_{\text{sgd}}H_{\text{eff}}^\top$ term) under the assumption of a sufficiently small learning rate at convergence, we obtain the continuous-time Lyapunov equation

$$H_{\text{eff}}C_{\text{sgd}} + C_{\text{sgd}}H_{\text{eff}}^\top \approx \eta\Sigma_\xi. \quad (70)$$

Taking the trace of both sides gives

$$\text{Tr}(H_{\text{eff}}C_{\text{sgd}}) + \text{Tr}(C_{\text{sgd}}H_{\text{eff}}^\top) \approx \eta\text{Tr}(\Sigma_\xi). \quad (71)$$

Using cyclicity of the trace and the symmetry of C_{sgd} , we have

$$\text{Tr}(C_{\text{sgd}}H_{\text{eff}}^\top) = \text{Tr}((C_{\text{sgd}}H_{\text{eff}}^\top)^\top) = \text{Tr}(H_{\text{eff}}C_{\text{sgd}}), \quad (72)$$

so that

$$\boxed{\text{Tr}(H_{\text{eff}}C_{\text{sgd}}) \approx \frac{\eta}{2}\text{Tr}(\Sigma_\xi)}. \quad (73)$$

Finally, we use the result from Appendix D.1 and D.2, and assuming that the Hessian is stable around the minimum w^* , which lies at the center of the SGD stationary dynamics, we have that TPV under SGD noise is given by,

$$\boxed{\text{Tr}(H_{\text{eff}}C_{\text{sgd}}) \approx \frac{\eta\sigma_\varepsilon^2}{2b}\text{Tr}(\nabla_w^2 L(w^*))} \quad (74)$$

where η and b are the SGD learning rate and batch size, and σ_ε^2 denotes the variance of the residual error over the training samples (assumed to be i.i.d.).

E. TPV for Parameter Quantization Noise

TPV is given by $\text{Tr}(H_{\text{eff}}C)$. We show in Appendix D.2 that $H_{\text{eff}}(w) \approx \nabla_w^2 L(w)$ (Hessian) near minima w^* . Under the quantization model above, the parameter perturbation covariance is $C_{\text{quant}} \approx \frac{\delta^2}{12}I_p$, where I_p is the identity matrix (thus obeying the TPV trace stability requirement), which proves the claim.

F. Experiments

F.1. Details of Experiments in Section 5.1

F.1.1. SYNTHETIC DATA EXPERIMENT:

For the synthetic experiments, we consider three families of data-generating processes: (i) a Gaussian linear teacher ($y = x^\top w_{\text{true}}$), (ii) a ReLU teacher ($y = \text{ReLU}(a^\top x)$), and (iii) a 10-unit multi-ReLU teacher ($y = \sum_{k=1}^{10} \text{ReLU}(a_k^\top x + b_k)$), each with isotropic inputs $x \sim \mathcal{N}(0, I_d)$. We sweep over three input dimensions $d \in \{10, 20, 50\}$ and two training-set sizes $n_{\text{tr}} \in \{10, 1000\}$. The test set always contains 5000 samples. For the student network, we use fully-connected ReLU MLPs with widths $w \in \{1, 256\}$ and depths $\{2, 3, 4\}$.

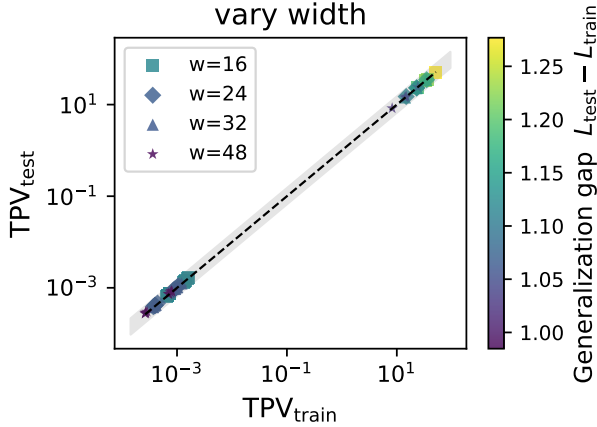


Figure 11. **TPV stability on CIFAR-100:** Analogous to Figure 1, this scatter plot shows that TPV stability holds for different width architectures on CIFAR-100.

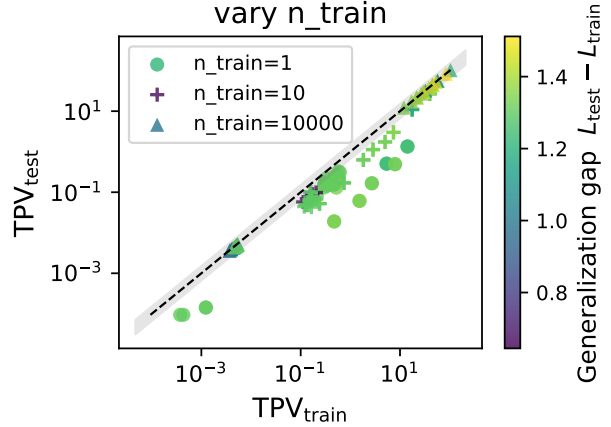


Figure 12. **TPV stability on CIFAR-100:** Analogous to Figure 4, this scatter plot shows that TPV stability breaks for very low values of n_{train} and holds increasing better (close to $y = x$ line and within the 50% error band) for larger values.

Clean reference model. For every configuration (dataset type, d , n_{tr} , w , depth), we train a clean reference network f_{w^*} on 1000 samples of noiseless training data using full-batch SGD with learning rate 2×10^{-3} , cosine-annealing LR schedule, momentum 0.9, no weight decay, and 800 training epochs. The resulting parameters w^* and predictions $f_{w^*}(x)$ on both train and test sets are cached and reused across all perturbation experiments.

Label-noise perturbations. For the label-noise experiments, we retrain from the fixed initialization w^* for $R = 20$ independent runs. Each run injects additive i.i.d. Gaussian noise $\varepsilon \sim \mathcal{N}(0, \sigma^2)$ with $\sigma \in \{0.005, 0.01\}$ to the clean labels. Each model is then trained for 200 epochs with full-batch GD, learning rate 2×10^{-3} , cosine annealing, momentum 0.9, and no weight decay. We record the empirical train/test TPV, train/test MSE, and a scalar first-order Taylor approximation error (described below). Empirical TPV is computed as

$$\widehat{\text{TPV}}_{\text{train}} = \frac{1}{Rn_{\text{train}}} \sum_{r=1}^R \sum_{i=1}^{n_{\text{train}}} \|f^{(r)}(x_i) - f^*(x_i)\|_2^2,$$

and analogously for the test set.

SGD-noise perturbations. To simulate stationary SGD noise around a minimum, we initialize the model at w^* and run SGD for 1000 steps with momentum 0.9 and no weight decay, using learning rates $\{10^{-3}, 5 \times 10^{-4}\}$ and batch sizes $\{32, 128\}$. The number of training samples n_{tr} may be as small as 10, so we disable `drop_last` in the PyTorch DataLoader to avoid degenerate cases with empty batches. Snapshots are collected every 20 steps after a burn-in period of 200 steps. Each snapshot is treated as a run and together, the deviation of the fine-tuned model logits from the clean (reference) model logits from these different runs give an estimate of empirical TPV using the same empirical TPV formula as above. We also track the Taylor approximation error.

First-order validity check. For every noisy model (label-noise run or SGD snapshot), we compute a relative finite-difference Taylor error to evaluate whether the model remains in a first-order regime around w^* . Let $\Delta = w - w^*$ and let $h = 10^{-2}$ be a finite-difference step. For a randomly-selected reference set of 128 training inputs X_{ref} , we estimate

$$\text{rel_err} = \frac{\mathbb{E}_{x \in X_{\text{ref}}} \left[(f_w(x) - f_{w^*}(x)) - \frac{f_{w^*+h\Delta}(x) - f_{w^*}(x)}{h} \right]^2}{\mathbb{E}_{x \in X_{\text{ref}}} [(f_w(x) - f_{w^*}(x))^2] + 10^{-12}},$$

where expectations are empirical averages over X_{ref} . We then discard the runs with values above the threshold 10^{-3} .

Total configuration count. We consider two experiment groups: (a) varying n_{tr} with fixed width, and (b) varying width with fixed n_{tr} . Taken together, the sweeps cover $3 \times 3 \times 2 \times 3 \times 2 = 108$ label-noise configurations and $3 \times 3 \times 2 \times 3 \times 4 = 216$

SGD-noise configurations, for a combined total of 324 distinct settings, each with up to 20 independent label-noise runs or ≈ 40 SGD-noise snapshots. These yield the TPV scatter plots in Fig. 1 and Fig. 2.

F.1.2. CIFAR EXPERIMENT

1. Vary Width Experiment Details:

We describe the details for the CIFAR-10 experiment in Fig 3 below. Details for CIFAR-100 (Fig. 11) are similar except the output has 100 dimensional logits and we use analogous CIFAR-100 pre-trained architectures.

Dataset and preprocessing. We use the standard CIFAR-10 per-channel normalization. From these, we randomly subsample $n_{\text{train}} = 10000$ and $n_{\text{test}} = 10000$.

Reference models. We use pre-trained mobilenetv2_x0.5, mobilenetv2_x0.75, mobilenetv2_x1_0, mobilenetv2_x1_4 from Pytorch Hub and denote its logits by $f^*(x)$. These models have widths roughly 16, 24, 32, 48 respectively.

Label-noise mechanism (logit noise). For the label-noise experiments, we retrain from the fixed initialization w^* for $R = 5$ independent runs. Each run injects additive i.i.d. Gaussian noise $\varepsilon \sim \mathcal{N}(0, \sigma^2)$ with $\sigma \in \{0.05, 0.1\}$ to the clean labels. Each model is then trained for 50 epochs using mini-batch SGD MSE regression on the noisy logits with momentum 0.9, learning rate 10^{-4} , batch size 256, and 0 weight decay. Mini-batch shuffling is turned off and a randomness seed is used so that each run sees the same sequence of mini-batches in order to avoid randomness due to SGD and focus only on randomness due to label noise. Also, we train the models in Pytorch eval mode so that modules like batch norm do not make output logits batch dependent. See Appendix C.3.4 for more details. We record the train/test CE (for generalization gap) and empirical train/test TPV using all these runs.

Empirical TPV is computed as

$$\widehat{\text{TPV}}_{\text{train}} = \frac{1}{Rn_{\text{train}}} \sum_{r=1}^R \sum_{i=1}^{n_{\text{train}}} \|f^{(r)}(x_i) - f^*(x_i)\|_2^2,$$

and analogously for the test set. We additionally record the cross-entropy loss on clean labels test set.

SGD-noise mechanism. To simulate stationary SGD noise around a minimum, we initialize the model at w^* and run SGD on the CIFAR-10 classification task using cross-entropy loss for 10 epochs with momentum 0.9 and no weight decay, using learning rates $\{10^{-4}, 5 \times 10^{-5}\}$ and batch sizes $\{128, 256\}$. Snapshots are collected every epoch. Each snapshot is treated as a run and together, the deviation of the fine-tuned model logits from the clean (reference) model logits from these different runs give an estimate of empirical TPV using the same empirical TPV formula as above.

2. Vary Number of Samples Experiment Details:

For the experiment with varying number of training samples (Fig. 4), we use pretrained ResNet-20/32/44/56 models on CIFAR-10. Notice these architectures have different depth, which is not a consideration in the TPV theory, and is merely used as a source of variation in our experiments. The experimental details are similar to the varying width experiment above, except now we group experiments by a randomly selected training dataset subset of size $n_{\text{train}} \in \{1, 10, 10000\}$.

For CIFAR-100, analogous pre-trained models are used corresponding to each of the CIFAR-10 models. All pretrained models are taken from the GitHub repository `chenyaofo/pytorch-cifar-models`.

F.2. Details of Experiments in Section 5.2

F.2.1. SYNTHETIC DATA EXPERIMENTAL SETUP

We study a controlled synthetic regression problem designed to empirically test Theorem 3.2. Inputs $x \in \mathbb{R}^{20}$ are drawn i.i.d. from $\mathcal{N}(0, I)$, and targets are generated by a fixed teacher $y = x^\top w_{\text{true}}$ with $w_{\text{true}} \sim \mathcal{N}(0, I)$. We sample $n_{\text{train}} = 1000$ training points and $n_{\text{test}} = 5000$ test points. The learner is a three-layer ReLU MLP (input \rightarrow width \rightarrow width \rightarrow 1), and we sweep over widths $\{128, 256, 512, 800, 1024, 1600\}$. For each width, we first train a ‘‘clean’’ reference network on the noiseless labels using full-batch SGD with momentum 0.9, fixed learning rate 5×10^{-3} , no weight decay, and 800 epochs. This gives a reference parameter w^* and corresponding reference outputs $f^*(x)$ on both the training and test sets.

At w^* , we compute the full Jacobian $J \in \mathbb{R}^{n_{\text{train}} \times P}$ via automatic differentiation (one row per input), perform an SVD $J = USV^\top$, and estimate the test-distribution Hessian surrogate H_{eff} by sampling test inputs and computing $G_{ii} =$

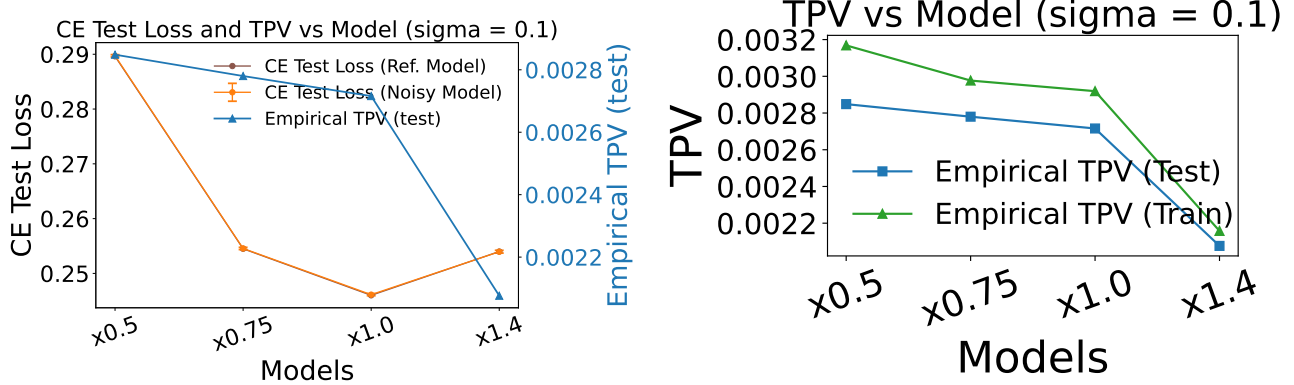


Figure 13. Empirical TPV estimates under target logit noise on CIFAR-10 for noise standard deviation $\sigma = 0.01$. Both TPV estimates reduce as width increases and correlate with the test set cross-entropy loss of the reference model.

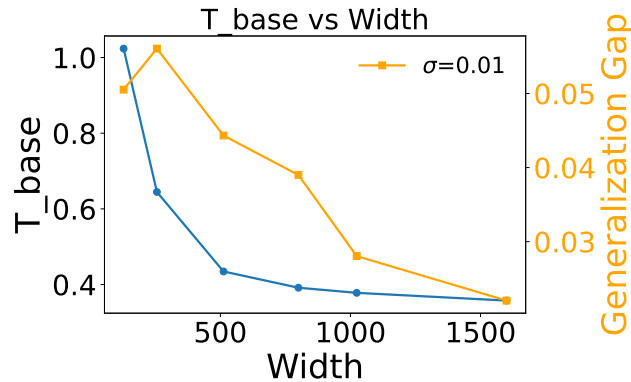


Figure 14. Generalization gap and T_{base} vs. network width. As width increases, both quantities reduce.

$\mathbb{E}_x[(g(x)^\top v_i)^2]$, where $g(x)$ is the gradient of the network output and v_i are the right singular vectors of J . The theoretical base quantity is then $T_{\text{base}} = \sum_i G_{ii}/s_i^2$, so that Theorem 3.2 predicts $\text{TPV} \approx \sigma^2 T_{\text{base}}$ for label-noise variance σ^2 .

To estimate empirical TPV, for each pair (width, σ) with $\sigma \in \{0.01, 0.05, 0.1, 0.2\}$, we run 50 independent Monte Carlo trials. In each trial we add i.i.d. noise $\epsilon \sim \mathcal{N}(0, \sigma^2)$ to the training labels, re-initialize the model at w^* , and retrain using identical optimization settings for 500 epochs, and no proximity penalty. Empirical TPV on train and test sets is computed as the variance across runs of the predictions relative to f^* .

F.2.2. CIFAR EXPERIMENTAL SETUP

We evaluate empirical TPV under injected Gaussian noise on the *logits* of a clean reference model on CIFAR-10/100. We describe the details for CIFAR-10 below. Details for CIFAR-100 are similar except the output has 100 dimensional logits.

Dataset and preprocessing. We use the standard CIFAR-10 per-channel normalization. From these, we randomly subsample $n_{\text{train}} = 4000$ and $n_{\text{test}} = 4000$. We find that it is important to use a sufficiently large samples size for consistent estimate.

Reference models. For each architecture in `cifar10_mobilenetv2_x0_5`, `cifar10_mobilenetv2_x0_75`, `cifar10_mobilenetv2_x1_0`, and `cifar10_mobilenetv2_x1_4`, we load a pretrained clean model from Pytorch Hub and denote its logits by $f^*(x)$. For every architecture, we compute the baseline cross-entropy losses on the clean labels for both train/test sets.

Label-noise mechanism (logit noise). For each model, we use Gaussian noise level $\sigma = 0.1$, and we run $R = 20$ Monte Carlo replicates. For each replicate, we sample noise

$$\varepsilon_i \sim \mathcal{N}(0, \sigma^2 I_{10}),$$

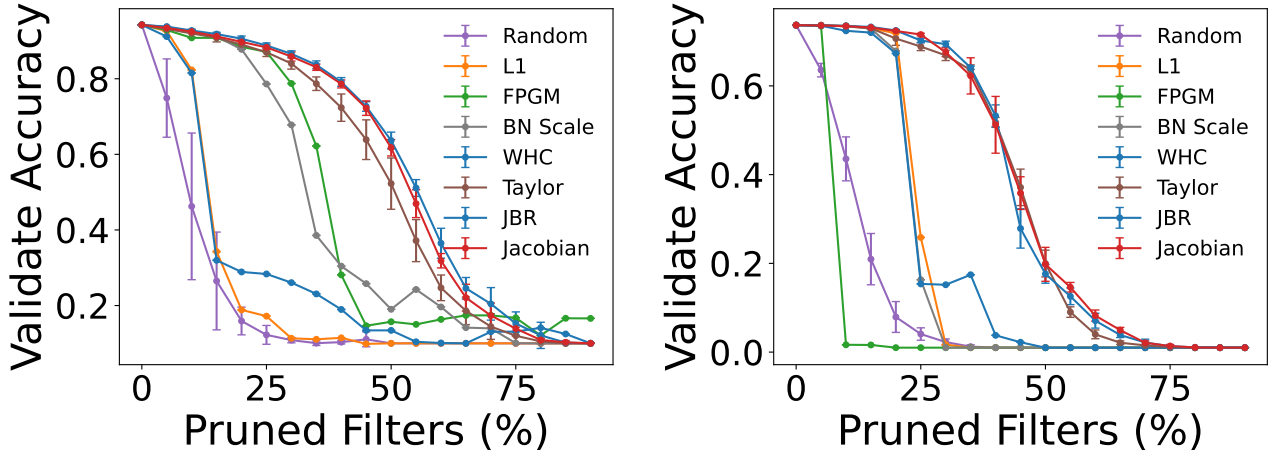


Figure 15. Pruning results of various criteria on Cifar-10 with ResNet-56 (left) and Cifar-100 with VGG-19 (right). JBR matches or outperforms existing methods.

and construct the noisy regression target using the randomly selected n_{train} samples in the training set as

$$y_i^{\text{noisy}} = f^*(x_i) + \varepsilon_i \quad (1 \leq i \leq n_{\text{train}}).$$

Noise-trained model. Each replicate begins by re-initializing the model to the clean reference weights w^* . We then fine-tune this model for 10 epochs using mini-batch SGD MSE regression on the noisy logits with momentum 0.9, learning rate 10^{-4} , batch size 256, and 0 weight decay. Mini-batch shuffling is turned off and a random seed is used so that each run sees the same sequence of mini-batches in order to avoid randomness due to SGD and focus only on randomness due to label noise. Also, we train the models in Pytorch eval mode so that modules like batch norm do not make output logits batch dependent. See Appendix C.3.4 for more details.

TPV estimation. After training each noisy model, we record its logits $f^{(r)}(x)$ on both train and test subsets. Empirical TPV is computed as

$$\widehat{\text{TPV}}_{\text{train}} = \frac{1}{Rn_{\text{train}}} \sum_{r=1}^R \sum_{i=1}^{n_{\text{train}}} \|f^{(r)}(x_i) - f^*(x_i)\|_2^2,$$

and analogously for the test set. We additionally record the cross-entropy loss on clean labels test set.

F.2.3. IMAGENET EXPERIMENTAL SETUP

For ImageNet, we use pre-trained `resnet50`, `resnet18`, `wide_resnet50_2`, `shufflenet_v2_x1_0`, `efficientnet_b0`, `mnasnet1_0`, `convnext_tiny` from Pytorch Hub. We randomly subsample $n_{\text{train}} = 10000$ and $n_{\text{test}} = 10000$. We use Gaussian noise level $\sigma = 0.01$, $R = 5$, and fine-tune this model for 10 epochs using mini-batch SGD MSE regression on the noisy logits with momentum 0.9, learning rate 10^{-6} , batch size 64, and 0 weight decay. While training, the loss is computed by summing the squared error over all the samples and logits in the mini-batch, but we track the MSE over samples. Additionally, it was extremely difficult to make the training loss go lower than the initial loss, and we had to turn on mini-batch shuffling within each run to make the loss go down. Nonetheless, we use a fixed random seed across runs so that the shuffling order remained the same across runs. We also tried experiments with pre-trained models `mobilenet_v2`, `densenet121`, and `squeezenet1_0`, but we were unable to make the MSE training loss go down for these models. All other details are identical to the above CIFAR experiments.

F.3. Pruning Experiment Details

This appendix provides the experimental details for the pruning results reported in Section 5.3. All pruning experiments follow the global structured pruning protocol introduced in *Optimal Brain Compression (OBC)* (Chen et al., 2025). Our implementation is based on the official GitHub code of (Chen et al., 2025) and extends the OBC framework by adding the TPV-motivated JBR importance criteria.

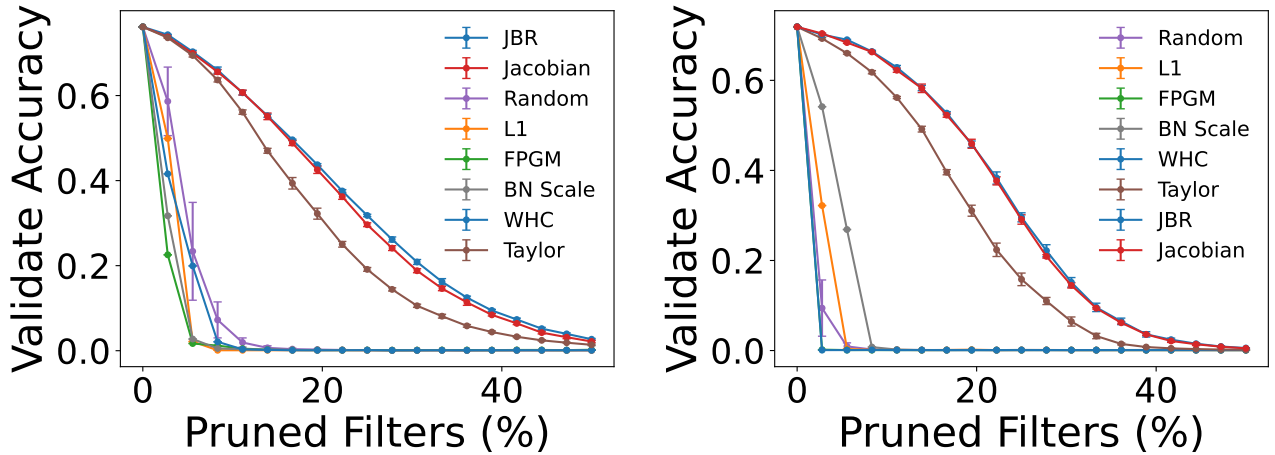


Figure 16. Pruning results of various criteria on ImageNet dataset using ResNet-50 (left) and MobileNet-v2 (right) without fine-tuning. JBR matches or outperforms existing methods.

F.3.1. PRUNING FRAMEWORK

We adopt the global channel-pruning pipeline of [Chen et al. \(2025\)](#). At each pruning iteration, an importance score is computed for every pruning group (typically convolutional or linear output channels, together with the corresponding input-channel dependencies). The least-important groups are removed globally, and the dependency graph ensures architectural consistency. No fine-tuning is performed between pruning iterations.

All pruning criteria evaluated in this work share the same dependency framework, pruning granularity, and iteration schedule. Thus, differences in accuracy arise solely from differences in importance scoring.

Fig. 15 and Fig. 16 show the same experiments as the ones in the main text, except the x-axis is now the percentage of pruned parameters.

F.3.2. MODELS AND DATASETS

We evaluate four standard classification settings:

- **ImageNet-1k:**
 - ResNet-50, pruned to 50% global channel sparsity.
 - MobileNet-V2, pruned to 50% global channel sparsity.
- **CIFAR-10:**
 - ResNet-56, pruned to 90% global sparsity.
- **CIFAR-100:**
 - VGG19-BN, pruned to 90% global sparsity.

F.3.3. PRUNING CRITERIA COMPARED

We compare the TPV-based **JBR** criterion with several established structured pruning criteria:

- **Jacobian** ([Chen et al., 2025](#)),
- **L1** weight-norm ([Li et al., 2017](#)),
- **Random** pruning,
- **BatchNorm scale** ([Liu et al., 2017](#)),

- **FPGM** (He et al., 2019) ,
- **WHC** (Chen et al., 2023),
- **Taylor** first-order saliency (Molchanov et al., 2019).

F.3.4. ITERATIVE PRUNING SCHEDULE

All pruning experiments use the following schedule:

- **Global pruning:** channel groups ranked and removed across the whole network.
- **Number of iterations:** 18.
- **Sparsity targets:**
 - 0.5 for ImageNet models,
 - 0.9 for CIFAR models.
- **Score recomputation:** importance scores recalculated at every iteration.
- **Data usage:**
 - 50 minibatches with batch size 256 for ImageNet scoring,
 - 50 minibatches with batch size 128 CIFAR datasets' scoring.

All reported scores are averaged over 5 independent pruning runs.